Parton Ladder Splitting and the Rapidity Dependence of Transverse Momentum Spectra in Deuteron-Gold Collisions at RHIC

Klaus WERNER [1], **Fu-Ming LIU** [2], **Tanguy PIEROG** [3]

[1] *SUBATECH, Université de Nantes – IN2P3/CNRS– EMN, Nantes, France*

[2] *Central China Normal University, Institute of Particle Physics, Wuhan, China*

[3] *Forschungszentrum Karlsruhe, Institut f. Kernphysik, Karlsruhe, Germany*

Abstract: We present a phenomenological approach (EPOS), based on the parton model, but going much beyond, and try to understand proton-proton and deuteron-gold collisions, in particular the transverse momentum results from all the four RHIC experiments. It turns out that elastic and inelastic parton ladder splitting is the key issue. Elastic splitting is in fact related to screening and saturation, but much more important is the inelastic contribution, being crucial to understand the data. We investigate in detail the rapidity dependence of nuclear effects, which is actually relatively weak in the model, in perfect agreement with the data, if the latter ones are interpreted correctly.

1 Introduction

Interesting new results have been observed in heavy ion collisions at RHIC, a large fraction of which being based on transverse momentum spectra. High transverse momenta seem to be suppressed [1, 2], systematically different for different hadron species [3].

But any quantitative expression of a suppression or an enhancement needs a reference, and here one usually refers to proton-proton scattering. Rather than working with the spectrum, one investigates the ratio R_{AA} of the nucleus-nucleus (AA) spectrum to the proton-proton (pp) result, the so-called nuclear modification factor,

$$R_{AA} = \frac{1}{N_{\rm coll}} \frac{dn^{AA}}{d^2p_t\, dy} \Big/ \frac{dn^{pp}}{d^2p_t\, dy}\,. \tag{1}$$

The normalization factor $1/N_{\rm coll}$ has been chosen such that at large transverse momenta one expects R_{AA} to become unity. Here, dn refers to the number of produced particles per inelastic interaction.

The first problem is therefore to understand sufficiently well proton-proton scattering. This is far from trivial. Experimentally, it is difficult to really access the full inelastic cross section, the interaction triggers tend to miss a more or less large fraction of the events. Theoretically, proton-proton is far from being fully understood, apart from perturbative calculations concerning very large transverse momenta.

A second problem arises due to the fact that even being sure about the observation of a non-trivial behavior of R_{AA}, we want to know whether this effect is really a collective one, providing evidence of the formation of a quark gluon plasma, and not something we observe already in proton-nucleus. This was the main purpose to study, in addition to gold-gold ($AuAu$), as well deuteron-gold (dAu) collisions at RHIC [4–8], with quite interesting results: the strong high p_t suppression in $AuAu$ seems to be absent in dAu, so we have clearly a final state effect.

Many features of dAu seem to be qualitatively understood, employing the saturation model [9–12], a recombination model [13], an improved parton model [14–16], the AMPT model [17]. But, what is really missing is a global and quantitative investigation: can we understand ALL the data presented so far by ALL the experiments, for pp and dAu, in a single approach. This gives also the opportunity to cross-check the different experiments, which is not so obvious to do directly.

The purpose of this paper is to present a phenomenological approach (EPOS), based on the parton model, but going much beyond, and try to understand pp and dAu, as far as the transverse momentum results from all the four RHIC experiments are concerned. It turns out that parton splitting (or better parton ladder splitting) is the key issue, which is related to screening and saturation, but there are other important consequences, which are crucial to understand the data.

2 Improved Parton Model with Remnants

The new approach we are going to present is called EPOS, which stands for

- ☐ **E**nergy conserving quantum mechanical multiple scattering approach, based on
- ☐ **P**artons (parton ladders)
- ☐ **O**ff-shell remnants
- ☐ **S**plitting of parton ladders

We are going to explain the different items in the following (the parton splitting will be discussed in a later section).

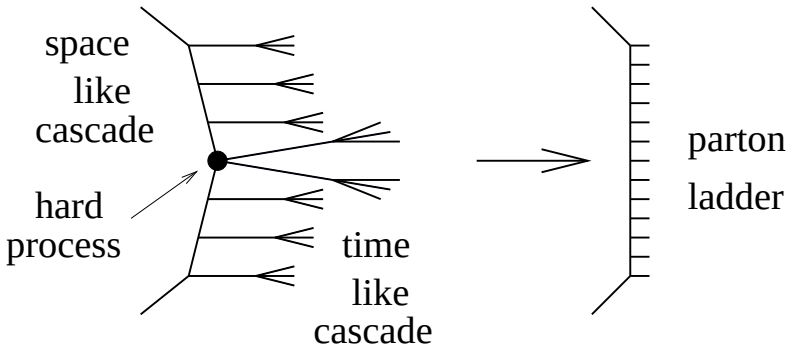

Figure **1**: Elementary parton-parton scattering: the hard scattering in the middle is preceded by parton emissions (initial state space-like cascade); these partons being usually off-shell, they emit further partons (final state time-like cascade). For all this we use a symbolic parton ladder.

One may consider the simple parton model to be the basis of hadron-hadron interaction models at high energies. It is well known that the inclusive cross section is given as a convolution of two parton distribution functions with an elementary parton-parton interaction cross section. The latter one is obtained from perturbative QCD, the parton distributions are deduced from deep inelastic scattering. Although these distributions are taken as black boxes, one should not forget that they represent a dynamical process, namely the successive emission of partons (initial state space-like cascade), which have to be considered in a complete picture. In addition, the produced partons are generally off-shell, giving rise again to parton emissions (final state time-like cascade). All this is sketched in fig. 1, where we also indicate that we refer to this whole structure as "parton ladder", with a corresponding simple symbol, to simplify further discussion.

For practical calculations, each parton ladder is finally translated into two color strings, which fragment into hadrons. This is a purely phenomenological procedure for the non-perturbative hadronization process.

Actually our "parton ladder" is meant to contain two parts: the hard one, as discussed above, and a soft one, which is a purely phenomenological object, parametrized in Regge pole fashion, for details see Appendix B.

Still the picture is not complete, since so far we just considered two interacting partons, one from the projectile and one from the target. These partons leave behind a projectile and target remnant, colored, so it is more complicated than simply projectile/target deceleration. One may simply consider the remnants to be diquarks, providing a string end, but this simple picture seems to be excluded from strange antibaryon results at the SPS [18].

We therefore adopt the following picture, as indicated in fig. 2: not only a quark, but a two-fold object takes directly part in the interaction, being a quark-antiquark, or a quark-diquark, leaving behind a colorless remnant, which is, however, in general excited (off-shell). So we have finally three "objects", all being white: the two off-shell remnants, and the parton ladders between the two active "partons" on either side (by "parton" we mean quark, antiquark, diquark, or antidiquark). We also refer to "inner contributions" (from parton

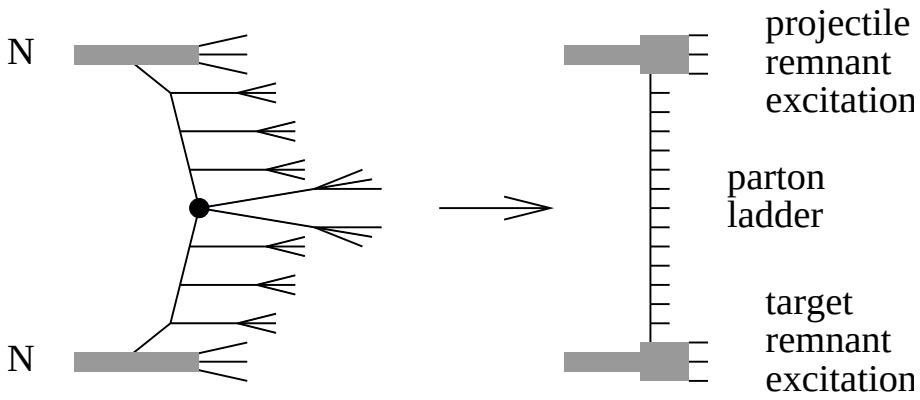

Figure **2**: The complete picture, including remnants. The remnants are an important source of particle production at RHIC energies.

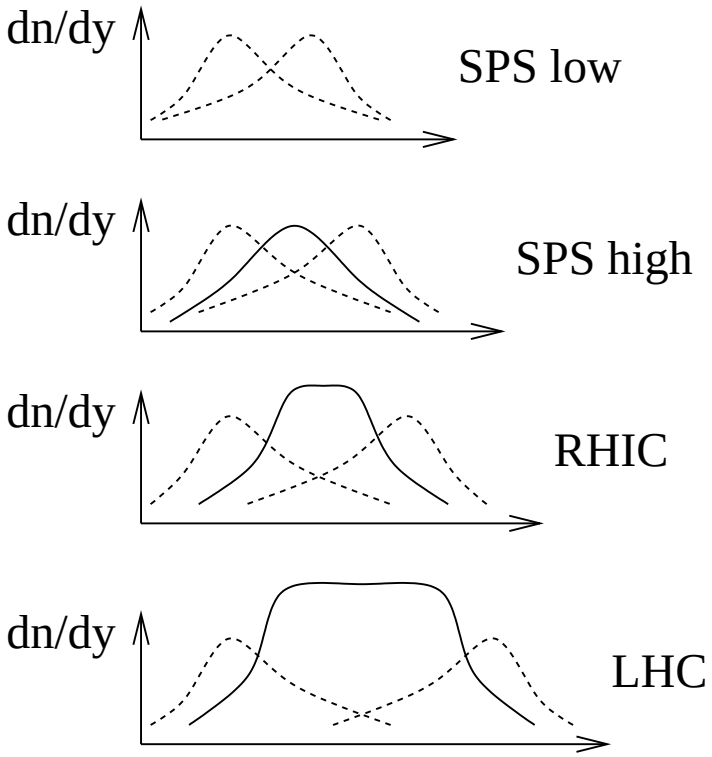

Figure **3**: Inner contributions, from the parton ladder (full lines), and "outer" contributions, from the remnants (dashed lines), to the rapidity distribution of hadrons. (Artists view)

ladders) and "outer contributions" (from remnants), reflecting the fact that the remnants produce particles mainly at large rapidities and the parton ladders at central rapidities, see fig. 3. Whereas the outer contributions are essentially energy independent, apart of a shift in rapidity, the inner contributions grows with energy, to eventually dominate completely central rapidities. But at RHIC, there is still a substantial remnant contribution at mid-rapidity.

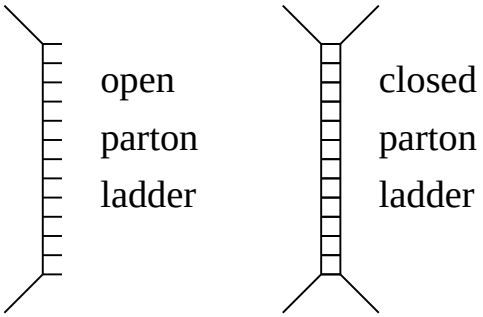

Figure **4**: The two elements of the multiple scattering theory: open ladders, representing inelastic interactions, and closed ladders, representing elastic interactions.

Even inclusive measurements require often more information than just inclusive cross sections, for example via trigger conditions. Anyhow, for detailed comparisons we need an event generator, which obviously requires information about exclusive cross sections (the widely used pQCD generators are not event generators in this sense, they are generators of inclusive spectra, and a Monte Carlo event is not a physical event). This problem is known since many years, the solution is Gribov's multiple scattering theory, employed since by many authors. This formulation is equivalent to using the eikonal formula to obtain exclusive cross sections from the knowledge of the inclusive one.

We indicated recently inconsistencies in this approach, proposing an "energy conserving multiple scattering treatment". The main idea is simple: in case of multiple scattering, when it comes to calculating partial cross sections for double, triple ... scattering, one has to explicitly care about the fact that the total energy has to be shared among the individual elementary interactions.

A consistent quantum mechanical formulation requires not only the consideration of the (open) parton ladders, discussed so far, but also of closed ladders, representing elastic scattering, see fig. 4. The closed ladders do not contribute to particle production, but they are crucial since they affect substantially the calculations of partial cross sections. Actually, the closed ladders simply lead to large numbers of interfering contributions for the same final state, all of which have to be summed up to obtain the corresponding partial cross sections. For details see appendix A.

We can do the complicated calculations, since we fit for example the result of a numerical calculation of a squared amplitude corresponding to a (open) parton ladder of energy $\sqrt{s}$, using a simple form αs^β, which allows then to perform analytical calculations. Furthermore, we employ very sophisticated Markov chain techniques to generate configurations according to multidimensional probability distributions. For details see appendix C and appendix D.

Important concerning numerical results: There are a couple of parameters which determine the parameterization of the soft elementary interaction (soft Pomeron), which are essentially fixed to get the pp cross sections right. The pQCD parameters (soft virtuality cutoff, K-factor, parton emission cutoff, parton-hadron coupling) are fixed to provide a reasonable parton distribution function

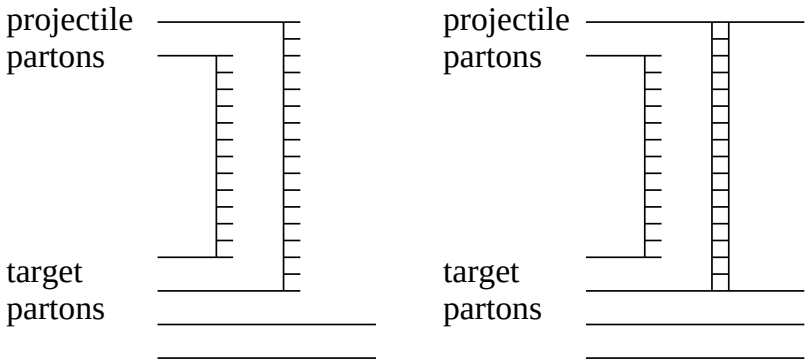

Figure **5**: Basic parton-parton interaction in nucleus-nucleus collisions: a projectile parton always interacts with exactly one parton on the other side, elastically (closed parton ladder) or inelastically (open parton ladder).

(which we calculate, it is not input!).

We assume the remnants to be off-shell with probability p_O, a mass distribution given as

$$\text{prob} \propto M^{-2\alpha_O}, \tag{2}$$

with parameter values which are not necessarily the same for diffractive and non-diffractive interactions (the latter ones being defined to be those without parton ladders). We use currently for p_O 0.75 (dif) and 0.95 (nondif), and for α_O 0.75 (dif) and 1.1 (nondif). Those excitation exponents may give rise to quite high mass remnants, RHIC and also SPS data seem to support this. High mass remnants will be treated as strings

There are four important fragmentation parameters: the break probability (per unit space-time area) p_B, which determines whether a string breaks earlier or later, the diquark break probability p_D, the strange break probability p_S, and the mean transverse momentum $\bar{p}_t$ of a break, with obvious consequences for baryon and strangeness production, and the p_t of the produced hadrons. We use three sets of these parameters, for the three types of strings: soft-, kinky(hard)-, remnant-strings. We do not really use the full freedom of these parameters, but one single set would not work – if we are interested in high precision. Somewhat surprising: p_S is 0.14 for soft and 0.06 for kinky strings. Maybe this reflects the fact that soft strings may have low masses, where strangeness is suppressed, and which needs some compensation. The parameter p_D is as well bigger for soft compared to kinky strings.

3 Splitting of Parton Ladders

Let us first consider very asymmetric nucleus-nucleus collisions, like proton-nucleus or deuteron-nucleus. The formalism developed earlier for pp can be generalized to these nuclear collisions, as long as one assumes that a projectile parton always interacts with exactly one parton on the other side, elastically or inelastically (realized via closed or open parton ladders), see fig. 5.

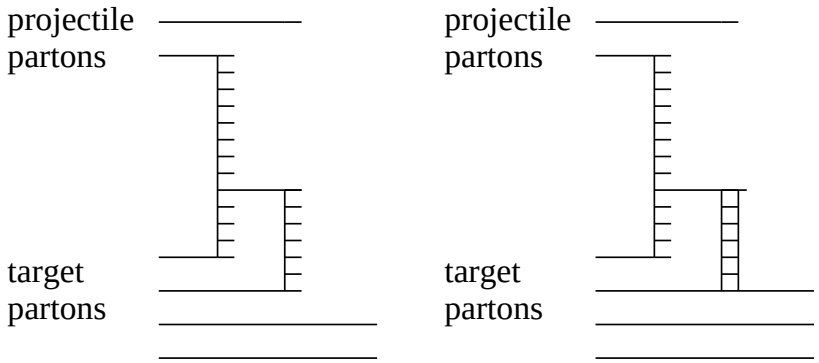

Figure **6**: Inelastic and elastic "rescattering" of a parton from the parton ladder with a second target parton. We talk about (inelastic and elastic) splitting of a parton ladder.

We employ the same techniques as already developed in the previous section. The calculations are complicated and require sophisticated numerical techniques, but they can be done. The corresponding results for dAu will be discussed later.

In case of protons (or deuterons) colliding with heavy nuclei (like gold), there is a complication, which has to be taken into account: suppose an inelastic interaction involving an open parton ladder, between a projectile and some target parton. The fact that these two partons interact implies that they are close in impact parameter (transverse coordinate). Since we have a heavy target, there are many target partons available, and among those there is a big chance to find one which is as well close in impact parameter to the two interacting partons. In this case it may be quite probable that a parton from the ladder interacts with this second target parton, inelastically or elastically, as shown in fig. 6.

Let us first discuss the effects of elastic splitting. The squared amplitude for an elementary inelastic interaction involving two partons with light cone momentum shares $x^+ = 2p^+/\sqrt{s}$ and $x^- = 2p^-/\sqrt{s}$ can be parametrized quite accurately as

$$\alpha\,(x^+)^\beta (x^-)^\beta, \tag{3}$$

with two parameters α and β depending on the squared energy s and the impact parameter b ($\sqrt{s}$ is the proton-proton cms energy). Any addition of an elastic contribution (closed ladder), be it in parallel or via splitting, provides an interference term, contributing negatively to (partial) cross sections. So an additional elastic leg, even though it does not affect particle production, it provides screening. Model calculations show that adding elastic splittings to the basic diagrams, modifies the corresponding squared amplitude as

$$\alpha\,(x^+)^\beta (x^-)^{\beta+\varepsilon},$$

and therefore the whole effect can be summarized by a simple positive exponent ε, which suppresses small light cone momenta. So the existence of many target partons effectively screens small x contributions, which agrees qualitatively with

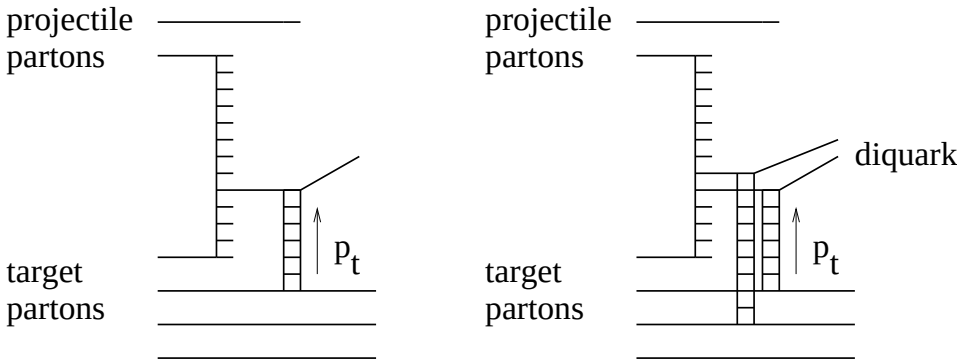

Figure **7**: Transport of transverse momentum via an attached closed ladder, which may be even enhanced in case of diquarks.

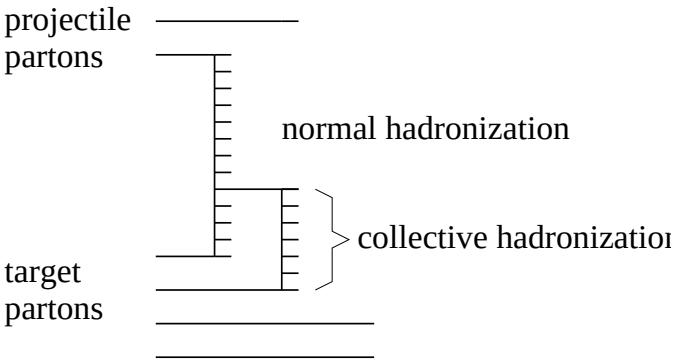

Figure **8**: Hadron production in case of inelastic ladder splitting.

the concept of saturation. But this is only a part of the whole story, several other aspects have to be considered.

One effect is the transport of transverse momentum via an attached closed ladder, as shown in fig. 7. Such a transport we use already in the basic parton model, when it comes to diffractive scattering, realized via a closed ladder. Here, some transverse momentum transfer is needed to explain the transverse momentum spectra of protons at large x (in the diffractive region). In case of diffractive target excitation, the projectile gets simply a p_t kick. We should have the same phenomenon in case of elastic splitting: the ladder parton involved in the interaction should get a p_t kick in the same way as the proton in diffractive scattering. This could be even more effective for diquarks (two attached ladders), leading finally to baryon production.

Let us turn to inelastic splitting, fig. 8 . Consider the example shown in the figure. In the upper part, there is only an ordinary parton ladder, so we expect "normal" hadronization. In the lower part, we have two ladders in parallel, which are in addition close in space, since they have a common upper end, and the lower ends are partons close in impact parameter, so the hadronization of the two ladders is certainly not independent, we expect some kind of a "collective" hadronization of two interacting ladders. Here, we only considered the most simple situation, one may also imagine three or more close ladders, hadronizing

collectively.

So far we discussed in a qualitative fashion the consequences of elastic and inelastic parton ladder splitting. The strength of the effects will certainly depend on the target mass, via the number Z of partons available for additional legs. The number Z of available partons will also increase with energy, so at high enough energy the above-mentioned effects can already happen in pp collisions.

4 Realization of Ladder Splitting Effects

The basic quantity for a numerical treatment of the ladder splitting effects is the number Z of partons available for additional legs, more precisely we have a Z_T for counting legs on the target side, and Z_P for counting legs on the projectile side. Let us treat Z_T (corresponding discussion for Z_P). Consider a parton in projectile nucleon i which interacts with a parton in target nucleon j. The number $Z_T(i,j)$ of addition legs has two contributions, one counting the legs attached to the same nucleon j, and one counting the legs attached to the other nucleons $j' \neq j$. We assume the following form:

$$\begin{aligned} Z_T(i,j) &= z_0 \, \exp(-b_{ij}^2/2{b_0}^2) + \\ &\quad + \sum_{\text{target nucleons } j' \neq j} z_0' \, \exp(-b_{ij'}^2/2{b_0}^2), \end{aligned}$$

where b_{ij} is the distance in impact parameter between i and j. The coefficients z_0 and z_0' depend logarithmically on the energy, as

$$\begin{aligned} z_0 &= w_Z \, \ln \, s/s_M \, , \\ z_0' &= w_Z \, \sqrt{(\ln \, s/s_M)^2 + {w_M}^2} \, , \end{aligned}$$

and the impact parameter width is $b_0 = w_B \, \sqrt{\sigma_{\text{inel}\,pp}/\pi}$, with parameters w_B, w_Z, w_M, and s_M. We then define

$$Z_T(j) = \sum_i Z_T(i,j).$$

We suppose that all the effects of the parton ladder splitting can be treated effectively, meaning that the correct explicit treatment of splittings is equivalent to the simplified treatment without splittings, but with certain parameters modified, expressed in terms of Z.

This is not only to simplify our life. Even an explicit dynamical treatment will stay a phenomenological approach, with many uncertainties, for example about the splitting vertices, and much more. So we prefer to have simple parameterizations rather than a very complicated but uncertain dynamical treatment.

So which quantities depend on Z, and how? In the following the symbols a_i are constants, used as fit parameters. The elastic splitting leads to screening, which is expressed by the screening exponents $\varepsilon = \varepsilon_S$ (for soft ladders) and $\varepsilon = \varepsilon_H$ (for hard ladders), and here we assume

$$\varepsilon_S = a_S \, \beta_S \, Z \, , \tag{4}$$

$$\varepsilon_H = a_H \, \beta_H \, Z \, , \tag{5}$$

where β_S and β_H are the usual exponents describing soft and hard amplitudes (see appendix C).

A second effect is transport of transverse momentum, here we suppose

$$\Delta p_t = a_T \, p_0 \, n_q \, Z, \tag{6}$$

where n_q is the number of quarks of the objects in the hadronization process (1 for quarks, 2 for diquarks), and $p_0 = 0.5$ GeV is just used to define a scale.

Let us come to the collective hadronization. We will actually "absorb" the multiple ladders into the remnants, which are usually treated as strings. Now we treat them as strings with modified string break parameters, to account for the collective hadronization. We modify the break probability (per unit space-time area) p_B, which determines whether a string breaks earlier or later, the diquark break probability p_D, the strange break probability p_S, and the mean transverse momentum $\bar{p}_t$ of a break, as

$$p_B \;\rightarrow\; p_B - a_B \, Z \, , \tag{7}$$

$$p_D \;\rightarrow\; p_D \, (1 + a_D \, Z) \, , \tag{8}$$

$$p_S \;\rightarrow\; p_S \, (1 + a_S \, Z) \, , \tag{9}$$

$$\bar{p}_t \;\rightarrow\; \bar{p}_t \, (1 + a_P \, Z) \, , \tag{10}$$

with positive parameters a_i. So with increasing Z, a reduced p_B will lead to more particle production, an increased p_D, p_S, $\bar{p}_t$, will lead to more baryon-antibaryon production, more strangeness production, and an increased p_t for each string break.

The parameters s_M, w_i, and a_i are chosen to reproduce mainly RHIC pp and dAu data, but also the energy dependence of cross sections and multiplicities from SPS to Tevatron. The best fit parameters are shown in table 1.

5 Results for Proton-Proton

Ladder splitting is quite important for pp at very high energies, where cross sections and multiplicities are considerably suppressed, due to screening. At RHIC energies, however, the effects are small: the total cross section is reduced by 5%, the multiplicity by 10%. Concerning the transverse momentum spectra to be discussed in detail in the following, the effect is hardly visible.

In order to compare to the charged particle p_t spectra in pp from the different experiments (STAR, PHENIX, BRAHMS), one has first to understand what has been measured. One wants to measure the inelastic differential yield,

$$\frac{d^3 n^{\rm inel}}{dy d^2 p_t} = \frac{1}{\sigma_{\rm inel}} \, \frac{d^3 \sigma^{\rm inel}}{dy d^2 p_t}, \tag{11}$$

where $\sigma \approx 42$ mb is the inelastic pp cross section, and $d^3\sigma^{\rm inel}/dyd^2p_t$ represents the inclusive differential cross section for inelastic events. In practice there is an

coefficient	corresponding variable	value
s_M	Minimum squared screening energy	(25 GeV)^2
w_M	Defines minimum for z_0'	6.000
w_Z	Global Z coefficient	0.080
w_B	Impact parameter width coefficient	1.160
a_S	Soft screening exponent	2.000
a_H	Hard screening exponent	1.000
a_T	Transverse momentum transport	0.025
a_B	Break parameter	0.070
a_D	Diquark break probability	0. 110
a_S	Strange break probability	0.140
a_P	Average break transverse momentum	0.150

Table **1**: Best fit values for splitting parameters. We included in the fit as well data not shown in this paper.

event trigger like the beam beam counter (BBC), which only counts a fraction of the events, missing in particular low multiplicity events.

UA5 [20] actually used a similar trigger to define non single diffractive (NSD) events. The NSD differential yield is given as

$$\frac{d^3n^{\rm NSD}}{dyd^2p_t} = \frac{1}{\sigma_{\rm NSD}}\frac{d^3\sigma^{\rm NSD}}{dyd^2p_t}, \tag{12}$$

where $\sigma \approx 35$ mb is the NSD pp cross section, and $d^3\sigma^{\rm NSD}/dyd^2p_t$ represents the inclusive differential cross section for NSD events. To be clear: NSD is not an absolute definition, it is defined via the acceptance of the UA5 detector! In figure 9, we show the corresponding pseudorapidity distribution for NSD events, slightly higher than the one for inelastic events. For the simulation of NSD events, we use simply the same requirement as used in the experiment (coincidence of charged particles in a forward and a backward pseudorapidity interval).

In case of STAR, one could as well define NSD as the events accepted by the BBC. Let us do so for the moment, and use the term NSD$^{\rm BBC}$. What is actually done is somewhat different. The differential cross section is multiplied by 30/26, in order to correspond to what Pythia defines to be non single diffractive, corresponding to 30mb. Let us call this NSD$^{\rm PYT}$. Actually the inelastic differential yield does not change, however, it is interpreted as spectrum for NSD$^{\rm PYT}$ events. Then again based on Pythia, it is argued that the inelastic differential yield for inelastic events is obtained essentially (with a small correction at small p_t) by multiplying with 30/42 (just the ratio of the cross sections), since SD events do not contribute to particle production. So after all, the originally measured differential yield (referring to NSD$^{\rm BBC}$) and the inelastic one differ essentially by a factor 42/30 = 1.4 – what is not at all what we observe, simulating NSD events with the BBC trigger condition, and comparing with inelastic events. As seen in fig. 10, the ratio of the NSD$^{\rm BBC}$ differential yield to the inelastic differential yield, rather than being 1.4, differs considerably as a function of p_t, and in addition depends on the particle species.

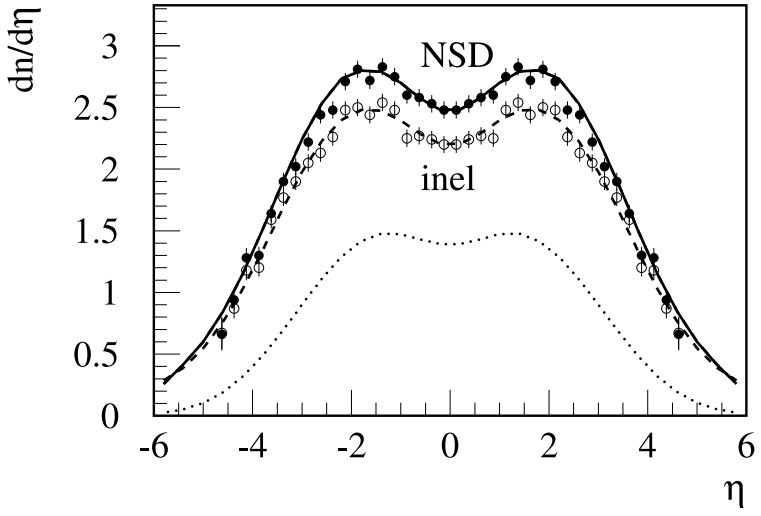

Figure **9**: Pseudorapidity distribution for inelastic and NSD events in pp collisions.The lines are EPOS results, the points data [20]. The dotted lined represents the "inner contribution" to the inelastic distribution (many particles are coming from remnants!).

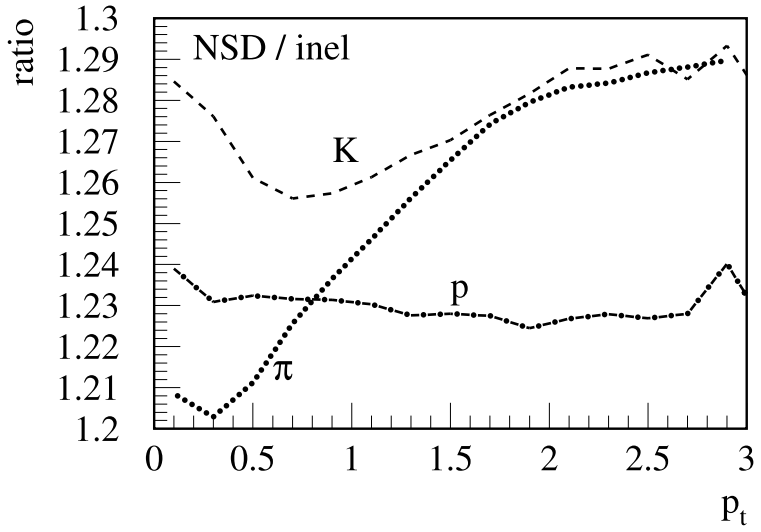

Figure **10**: Ratio of the NSD$^{\rm BBC}$ differential yield to the inelastic differential yield, in pp collisions, for a pions (π), kaons (K), and protons (p).

Based on the above discussion, we will simulate NSD$^{\rm BBC}$ differential spectra (we actually get exactly 26 mb for the NSD$^{\rm BBC}$ cross section), and compare with STAR's published NSD results, since they are identical to the NSD$^{\rm BBC}$ differential spectra. In this way we avoid all these problems related to Pythia correction procedures. In the following, NSD refers always to NSD$^{\rm BBC}$.

In fig. 11, we show p_t spectra for NSD events, compared to STAR data [21], and inelastic events, compared to PHENIX data [6, 22]. Simulation and data agree within 15% (over 6 orders of magnitude). This good agreement is only possible after our re-interpretation of NSD, see the discussion above.

When studying (later) dAu collisions, there will be plenty of discussion con-

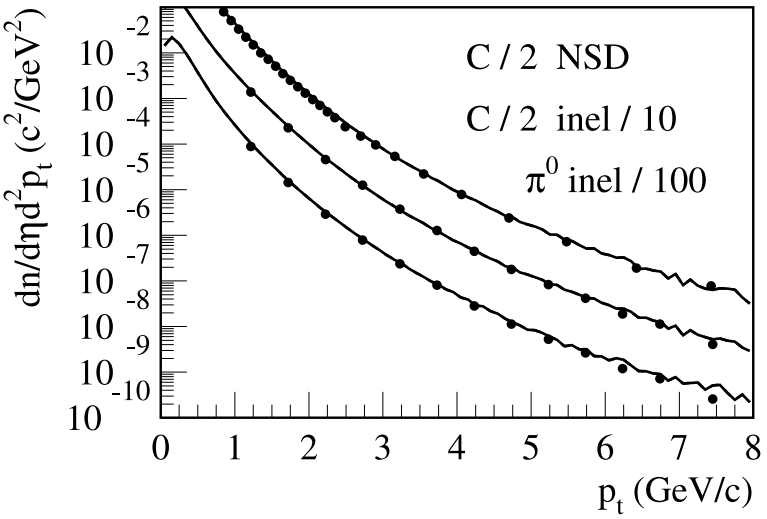

Figure **11**: Differential yields in pp collisions as a function of p_t, for (from top to bottom) charged particles (over 2) for NSD events, charged particles (over 2) for inelastic events, and neutral pions for inelastic events. Lines are EPOS simulations, points are data from STAR [21] and PHENIX [6, 22]. The two agree within 15% (over 6 orders of magnitude).

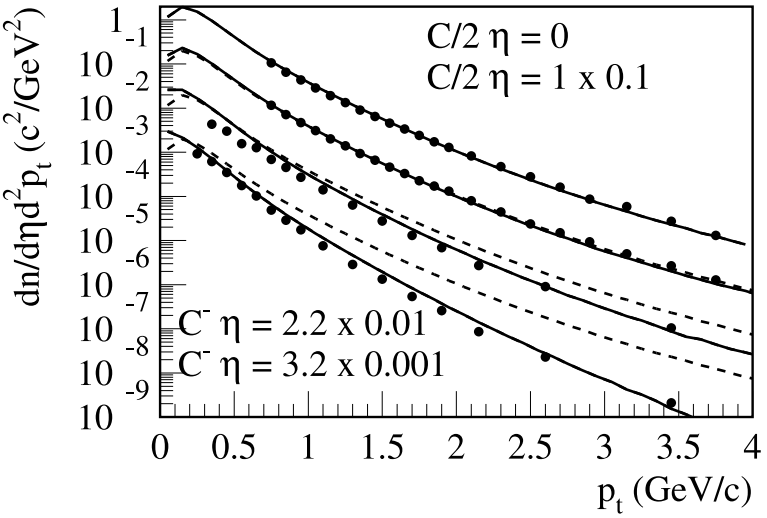

Figure **12**: Inelastic differential yields in pp collisions as a function of p_t, for (from top to bottom) charged particles (over 2) at $\eta = 0$, at $\eta = 1$, negative particles at $\eta = 2.2$, at $\eta = 3.2$ (always displaced by factors of 10). Lines are EPOS simulations, poins are data [7]. We also plot (dashed) the simulation curve at $\eta = 0$, multiplied by 0.1, 0.01, 0.001, to have a reference.

cerning the (pseudo)rapidity dependence of certain effects. It is therefore necessary to first check the (pseudo)rapidity dependence of p_t spectra for pp. In fig. 12, we plot inelastic differential yields as a function of p_t, at different pseudorapidities; $\eta = 0$, $\eta = 1$, $\eta = 2.2$, and $\eta = 3.2$ We show EPOS simulations compared to BRAHMS data [7]. We also plot (dashed) the simulation curve at $\eta = 0$, multiplied by 0.1, 0.01, 0.001, to have a reference for the results at the other pseudorapidi-

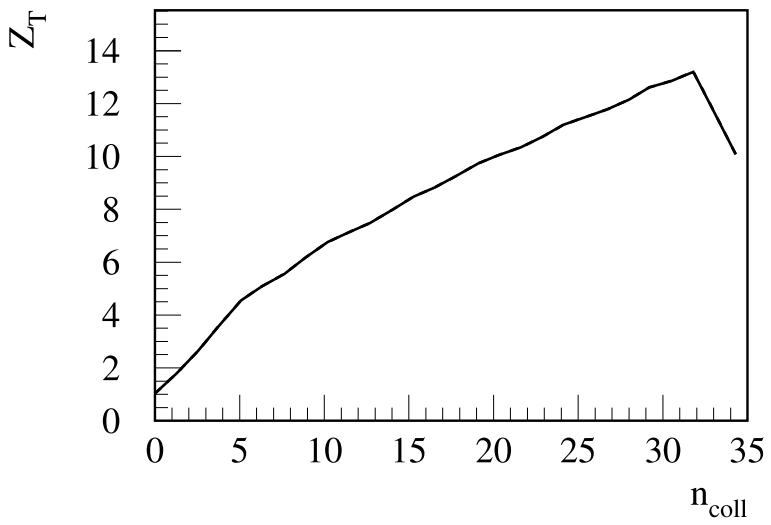

Figure **13**: The target Z as a function of centrality, expressed in terms of the number of binary collisions, for dAu.

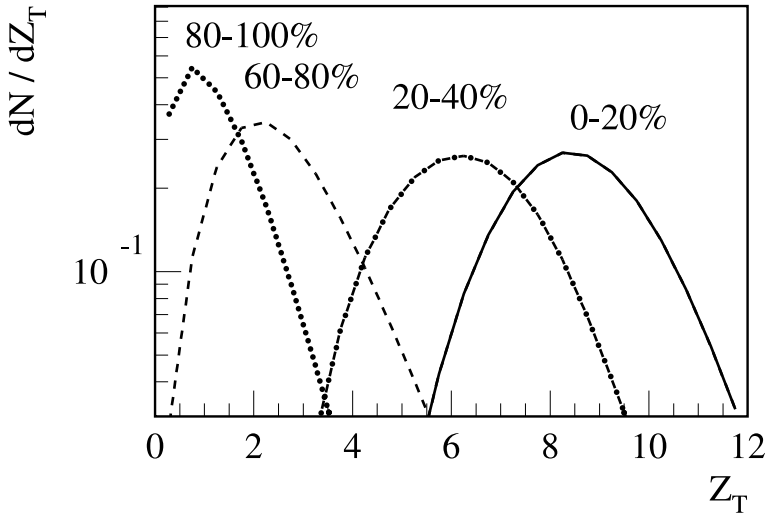

Figure **14**: The Z distribution, for different centrality classes.

ties. The spectra clearly get softer with increasing η.

6 Results Deuteron-Gold

All screening effect are linear in Z, so it is worthwhile to first investigate Z. In very asymmetric collisions as dAu, the projectile Z is essentially zero, whereas the target Z differers considerably from zero. As show in fig. 13 (and obvious from the definition) Z_T increases linearly with the number of collisions. So Z is essentially a centrality measure. In fig. 14, we show the Z distribution for the different centrality classes. In this way one understands easily how the different centrality classed are affected by the splitting effects.

Although we are mainly interested here in transverse momentum spectra,

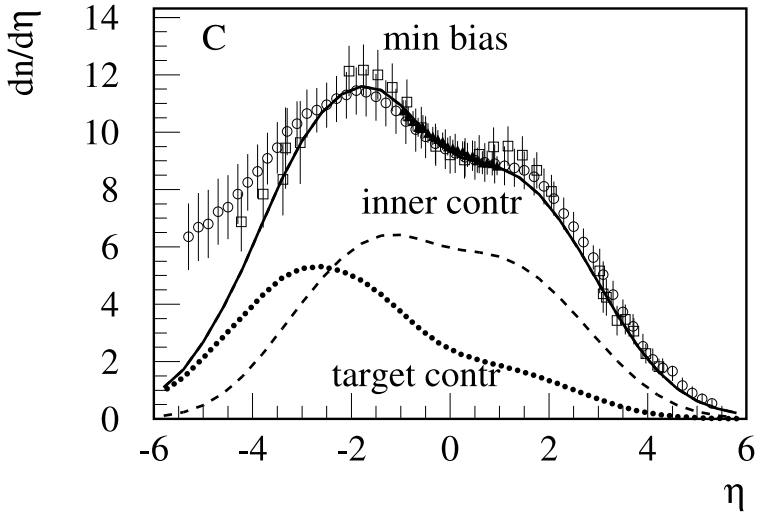

Figure **15**: Pseudorapidity spectra in minimum bias dAu collisions. Lines are EPOS simulations, points are data from PHOBOS [23] (circles), STAR [4] (triangles), BRAHMS [24] (squares). We also show the inner and the outer target contributions to the simulated distribution.

we still show first of all the pseudorapidity spectra, which finally determine the normalization of the p_t spectra. In fig. 15, we show pseudorapidity spectra in minimum bias dAu collisions: EPOS simulations, compared to data from from PHOBOS [23], STAR [4], and BRAHMS [24]. We also show different contributions to the simulated distribution. We distinguish inner and outer (projectile and target) contributions, where the outer contributions are meant to contain the multiple ladders, originating from ladder splittings, treated in a "collective" way, as discussed above. The inner contribution comes from ordinary ladders in the middle. The asymmetry of the distribution is clearly due to to the target contribution (the projectile contribution, not shown, is very small). Also not shown here is the result for "no splitting"; for central collisions, ladder splitting leads to an overall reduction of $dn/d\eta$ of about 30%. This is due to the fact that first of all the two splitting effects "screening" and "string break delay" are relatively small, and secondly work in opposite direction. In figs. 16 and 17, we show pseudorapidity spectra for central and peripheral dAu collisions.

Let us now turn to p_t spectra. One of the first observations concerning p_t spectra in dAu collisions was the fact that not only the nuclear modification factor shows a non-trivial behavior, but this behavior seems also to be strongly pseudorapidity dependent, even when varying η only by one unit. We want to investigate this question in the following.

In fig. 18, we show transverse momentum spectra of charged particles in dAu collisions at different centralities and at different pseudorapidities. The four figures represent minimum bias, central ($0-20\%$), mid-central ($20-40\%$) , and peripheral ($40-100\%$) collisions. For each figure, spectra for four pseudorapidity intervals are shown: $[-1,-0.5]$, $[-0.5,0]$, $[0,0.5]$, $[0.5,1]$. We simply refer to the corresponding mean values, $\eta=-0.75$, $\eta=-0.25$, $\eta=0.25$, $\eta=0.75$. For better visibility, the different curves have been displaced by factors of 10. Solid lines

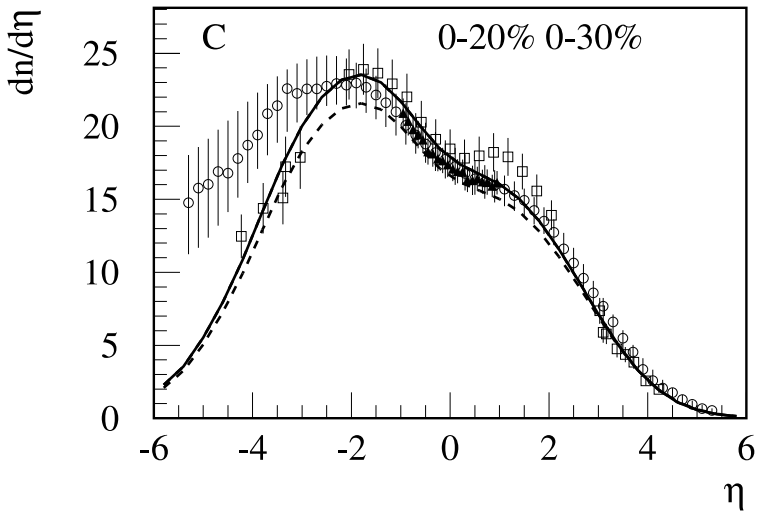

Figure **16**: Pseudorapidity spectra for central dAu collisions. Solid lines are EPOS simulations for 0-20%, dashed lines are simulations for 0-30%. Points are data from PHOBOS [25] (circles), STAR [4] (triangles), BRAHMS [24] (squares).

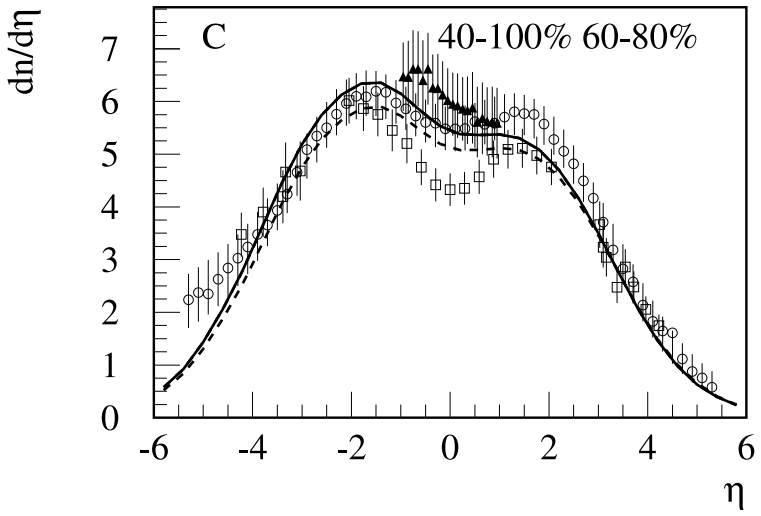

Figure **17**: Pseudorapidity spectra for peripheral dAu collisions. Solid lines are EPOS simulations for 40-100%, dashed lines are simulations for 60-80%. Points are data from PHOBOS [25] (circles), STAR [4] (triangles), BRAHMS [24] (squares).

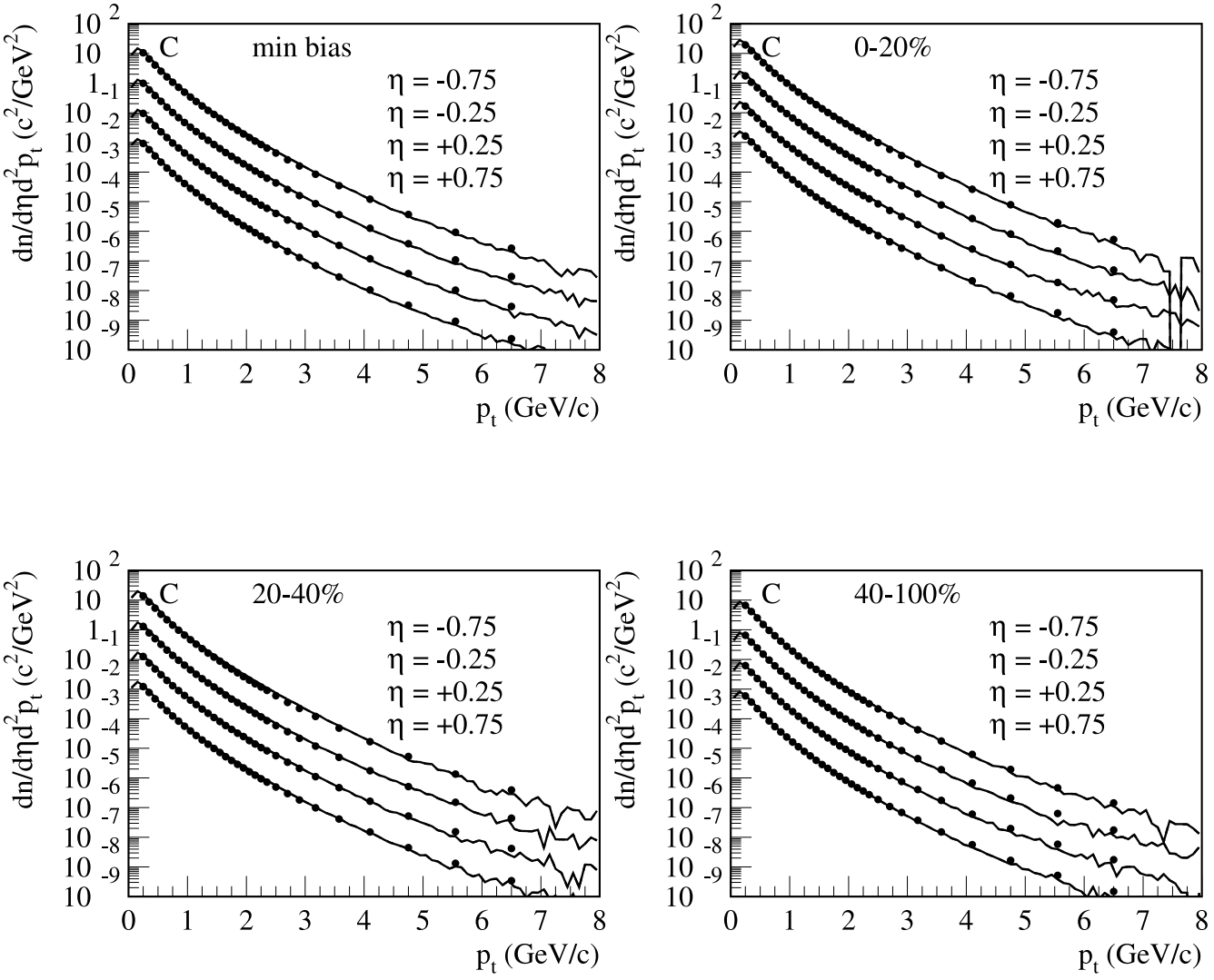

Figure **18**: Transverse momentum spectra of charged particles in dAu collisions at different centralities and at different pseudorapidities. The four figures represent minimum bias, central ($0-20\%$), mid-central ($20-40\%$) , and peripheral ($40-100\%$) collisions. For each figure, from top to bottom: $\eta = -0.75$, $\eta = -0.25$, $\eta = 0.25$, $\eta = 0.75$. Solid lines are EPOS simulations, points are data [4]. The different curves have been displaced by factors of 10.

are EPOS simulations, points are data [4], both agree within 10-20%. Although looking directly at spectra does not really allow to see systematic differences between the different curves, it is still useful to first check that the absolute curves agree, before investigating ratios.

To observe any "anomalous" behavior, one usually plots ratios, like the nuclear modification factor, defined earlier. The disadvantage is the fact that the corresponding pp spectrum has to be known, with a sufficient precision. An

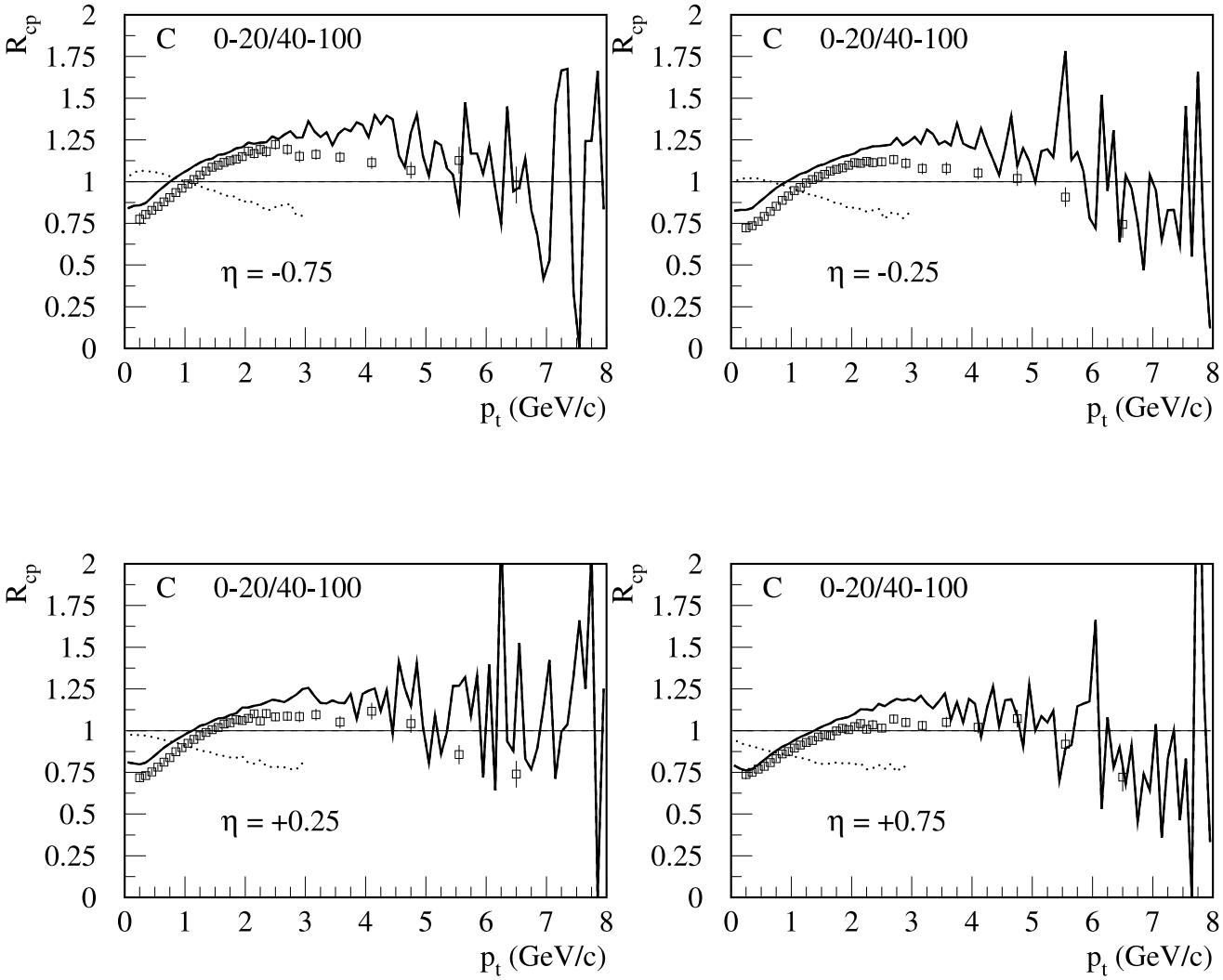

Figure **19**: R_{cp} ratios at different pseudorapidities ($\eta = -0.75$, $\eta = -0.25$, $\eta = 0.25$, $\eta = 0.75$). Solid lines are EPOS simulations, points are data [4]. The dotted lines are EPOS simulations, with parton ladder splitting turned off.

alternative procedure is the use of ratios of central to peripheral results,

$$R_{cp} = \frac{1}{N_{\rm coll}^{\rm central}} \frac{dn^{\rm central}}{d^2p_t\, dy} \Big/ \frac{1}{N_{\rm coll}^{\rm peripheral}} \frac{dn^{\rm peripheral}}{d^2p_t\, dy}\,. \tag{13}$$

In fig. 19, we show the R_{cp} ratios at different pseudorapidities ($\eta = -0.75$, $\eta = -0.25$, $\eta = 0.25\eta = 0.75$). Here, central refers to $0 - 20\%$ and peripheral to $40 - 100\%$. Solid lines are EPOS simulations, points are data [4]. We also show the corresponding EPOS results, with parton ladder splitting turned off. These curves are cut off at $p_t = 3$ GeV/c, to avoid that the strong statistical fluctuations spoil the figure. The no-parton-ladder-splitting curve increases slowly with p_t, in the shown range it stays well below one. It will finally reach one. The full EPOS simulations show quite a different behavior, the ratio R_{cp} increases

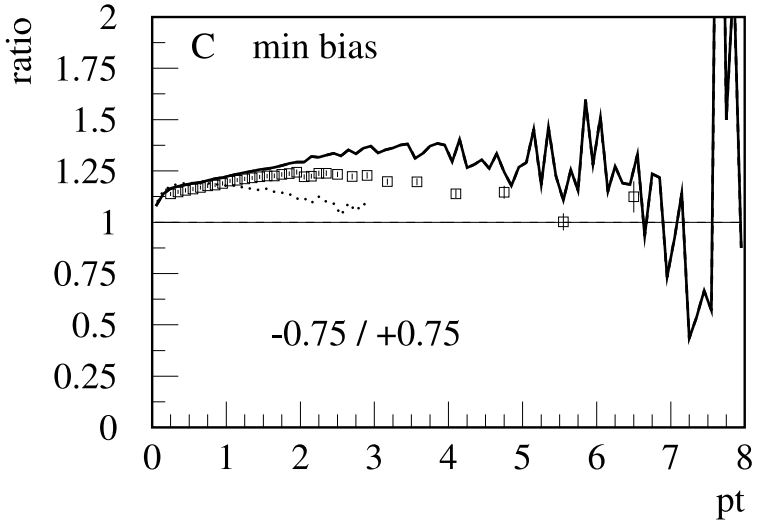

Figure **20**: Ratio of charged particle spectra at backward to forward pseudorapidities ($\eta = -0.75/\ \eta = 0.75$), in minimum bias dAu collisions. Solid lines are EPOS simulations, points are data [4]. The dotted lines are EPOS simulations, with parton ladder splitting turned off.

strongly between 1 and 2 GeV/c, to stay constant (or decrease) beyond. The statistical fluctuations do not really allow very precise predictions beyond 4 GeV/c. The strong increase between 1 and 2 GeV/c is due to collective hadronization on the target side, which leads to an increased transverse momentum production. As can be seen from fig. 15, target side hadronization extends even to forward pseudorapidities, so it is quite visible in the whole η range [-1,1]. The effect is simply somewhat stronger at backward compared to forward rapidity, since target hadronization contributes more. But the difference is not so big. The increase of R_{cp} with p_t is partly also due to the momentum transfer from the elastic splitting, which should affect equally backward and forward pseudorapidities. The variation of the shape of R_{cp} with pseudorapidity is quite small, the main modification is actually an overall factor due to the fact, that the particle density increases towards smaller pseudorapidities, as seen from fig. 15.

A direct way to investigate the pseudorapidity dependence of spectra is provided by the ratio of spectra at backward to forward pseudorapidities, like $\eta = -0.75/\ \eta = 0.75$, as shown in fig. 20. Here, one observes a slight increase between 0 and 2 GeV/c. This means that the R_{cp} at backward pseudorapidity increases a bit more than the one at forward pseudorapidity, which we understand such that there is somewhat more target side collective hadronization at backward pseudorapidity.

We now consider an even larger pseudorapidity variation: we investigate how the nuclear modification factors vary in the pseudorapidity range 0 to 3.2. Before comparing to data, we show the results of full EPOS simulations, as well as those with parton ladder splitting turned off. In fig. 21, we show the nuclear modification factors for charged particles in minimum bias dAu collisions, at different pseudorapidities: $\eta = 0$, $\eta = 1$, $\eta = 2.2$, $\eta = 3.2$. Whereas the no-splitting curves hardly change with p_t, and decrease with pseudorapidity, the full calculations

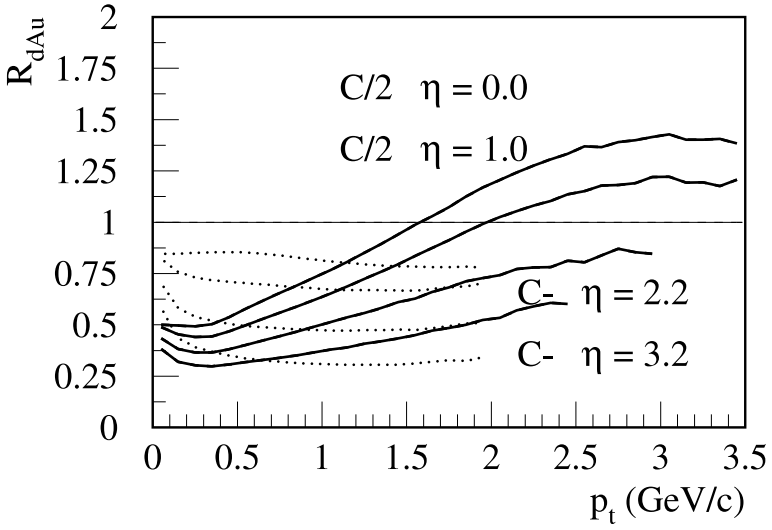

Figure **21**: Nuclear modification factors R_{dAu} for charged particles in minimum bias dAu collisions, at different pseudorapidities: $\eta = 0$, $\eta = 1$, $\eta = 2.2$, $\eta = 3.2$ (from top to bottom). The solid lines are full EPOS simulations, the dotted lines are EPOS with parton ladder splitting turned off.

show of course the same decrease with pseudorapidity, but all curves increase substantially with p_t between 1 and 3 GeV/c. This confirms the observation already made earlier by studying the variation in the η range -1 to 1.

In the following we will compare the simulations with data from all the four RHIC experiments. In fig. 22, we collect all published data on charged particle nuclear modification factors in minimum bias dAu collisions at (or close to) $\eta = 0$, together with the corresponding simulations. We show minimum bias results at $\eta = 0$ from STAR [5], at $\eta = 0.4$ from PHOBOS [8], 0-88% centrality results at $\eta = 0$ from PHENIX [6], and minimum bias data at $\eta = 0$ from BRAHMS [7]. We also show minimum bias EPOS simulations at $\eta = 0$, at $\eta = 0.4$, not feed down corrected minimum bias simulations, and 0-88% centrality results at $\eta = 0$. We first of all observe that the different simulation results are quite close to each other, so changing slightly the pseudorapidity, the centrality definition, doing or not feed down corrections, does not affect the final result too much. The variation of the experimental data is much bigger. On the upper end we have the STAR data, but based on the above discussion on pp results, we expect that the pp reference spectrum is 10-20% too low, which means R_{dAu} is 10-20% too high. The corresponding reduction would bring the STAR data down to the EPOS simulation curve (full line), and agree with the PHENIX data, and with the PHOBOS data. BRAHMS is on the lower end, but within the error bars compatible with the simulation curve.

In fig. 23, we consider charged particle nuclear modification factors in minimum bias dAu collisions at (or close to) $\eta = 1$, together with the corresponding simulations. We show minimum bias data at $\eta = 0.8$ from PHOBOS [8], at $\eta = 1$ from BRAHMS [7]. We also show minimum bias EPOS simulations at $\eta = 1$, at $\eta = 0.8$, both being very close to each other. The data are somewhat lower, but the curves are within the error bars. A systematic difference may again be due

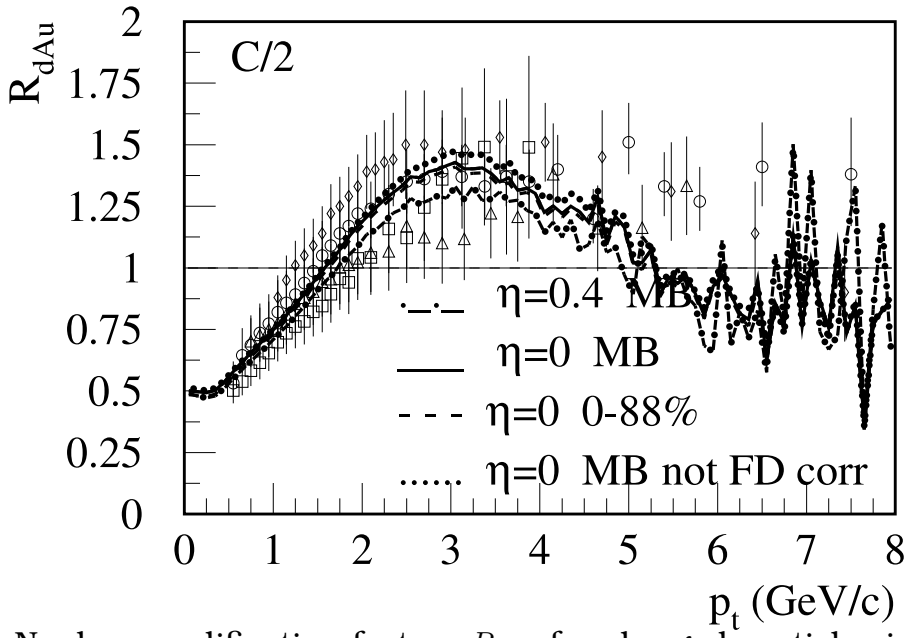

Figure **22**: Nuclear modification factors R_{dAu} for charged particles in minimum bias dAu collisions at (or close to) $\eta = 0$. The different lines are full EPOS simulations: minimum bias at $\eta = 0$ (full), at $\eta = 0.4$ (dashed-dotted), not feed down corrected (dotted), 0-88% centrality, at $\eta = 0$ (dashed). The points are minimum bias data at $\eta = 0$ from STAR [5] (rhombs), at $\eta = 0.4$ from PHOBOS [8] (squares), 0-88% centrality data at $\eta = 0$ from PHENIX [6] (circles), minimum bias results at $\eta = 0$ from BRAHMS [7] (triangles).

to the pp reference. To investigate this, we also plot a "mixed" R_{dAu}: the nuclear spectrum is taken from BRAHMS, but we use the EPOS pp reference. The result (squares) now exceeds the simulation curve.

In fig. 24, we finally compare EPOS simulations and data from BRAHMS [7] at $\eta = 2.2$ and $\eta = 3.2$. Data and simulations agree quite well.

7 Summary

In this paper, we have presented a phenomenological approach, called EPOS, based on the parton model, but going much beyond. There are two very important "nuclear effects": elastic and inelastic parton ladder splitting, which in principle occurs already in pp scattering, but which becomes really visible when systems with large numbers of partons (like nuclei) are involved.

Elastic splitting is in fact related to screening and saturation, but much more important is the inelastic contribution, being crucial to understand the data.

The main effect (at least concerning the observables investigated in this paper) is due to the fact that inelastic splitting (bifurcation of parton ladders), leads to a modified hadronization process, a "collective hadronization" of multiple, parallel parton ladders, on the target side, in case of dAu. This is the equivalent of string fusion, if one uses the language of strings. But contrary to the usual string fusion picture, here we do not have complete ladders which behave collectively, but only the bifurcated ones on the target side.

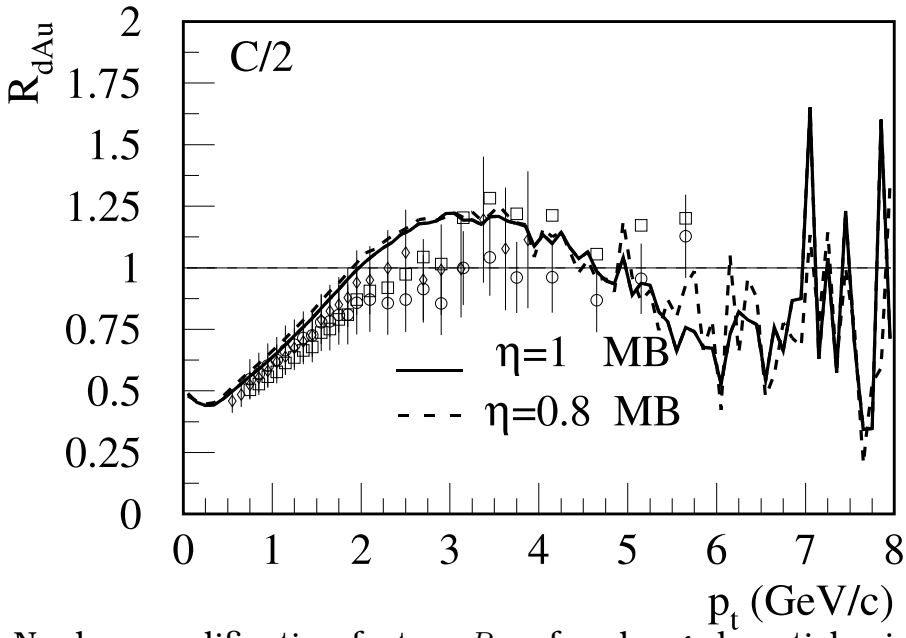

Figure **23**: Nuclear modification factors R_{dAu} for charged particles in minimum bias dAu collisions at (or close to) $\eta = 1$. The different lines are full EPOS simulations: minimum bias at $\eta = 1$ (full), at $\eta = 0.8$ (dashed). The points are minimum bias data at $\eta = 0.8$ from PHOBOS [8] (rhombs), at $\eta = 1$ from BRAHMS [7] (circles). The squares represent R_{dAu} calculated from the BRAHMS dAu p_t spectrum and the pp simulation result.

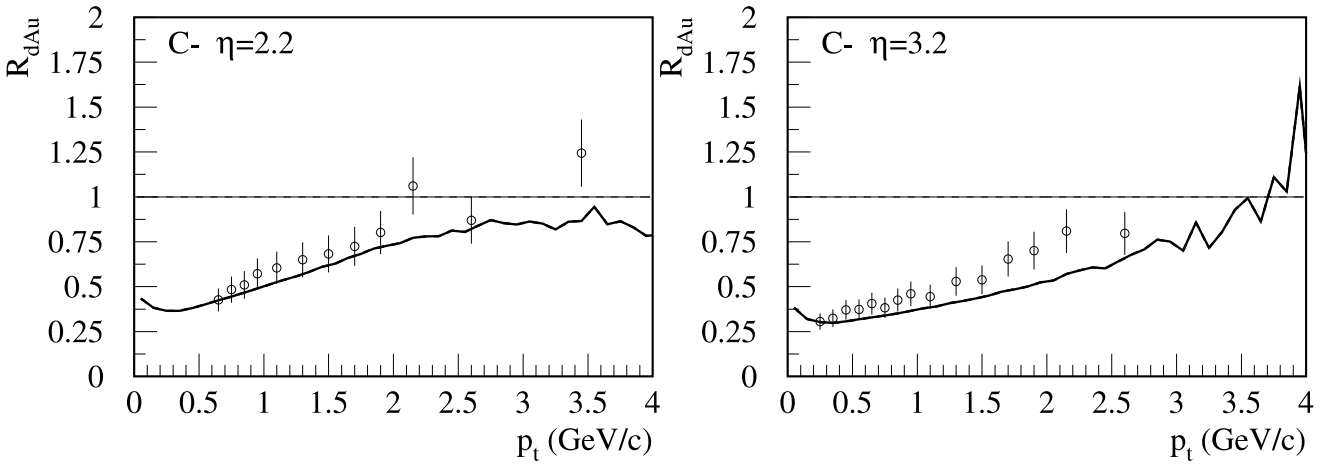

Figure **24**: Nuclear modification factors R_{dAu} for charged particles in minimum bias dAu collisions at $\eta = 2.2$ (left) and $\eta = 3.2$ (right). The lines are full EPOS simulations, the points are data from BRAHMS [7].

Concerning p_t spectra, the main effect of the collective hadronization is a p_t broadening. This is certainly what is needed, but real evidence for our picture can only come from a very detailed comparison with all corresponding data currently available. For this purpose we considered all published nuclear modification factor data, concerning charged particles, from all the four RHIC experiments.

We investigated in detail the rapidity dependence of nuclear effects, which is actually relatively weak in the model, in perfect agreement with the data, if the latter ones are interpreted correctly, and if one considers really ALL available data, and not just a convenient subset.

A Appendix on Multiple Scattering Theory

We first consider inelastic proton-proton scattering. We imagine an arbitrary number of elementary interactions to happen in parallel, where an interaction may be elastic or inelastic. The inelastic amplitude is the sum of all such contributions,

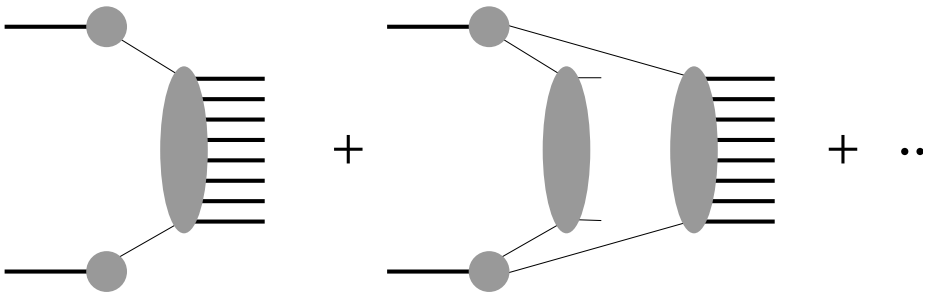

with at least one inelastic elementary interaction involved. To calculate cross sections, we need to square the amplitude, which leads to many interference terms, like for example

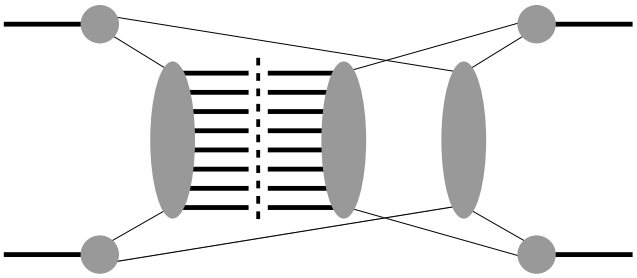

which represents interference between the first and the second diagram of the above-mentioned sum of terms. Using the above notations, we may represent the left part of the diagram as a cut diagram, conveniently plotted as a dashed line:

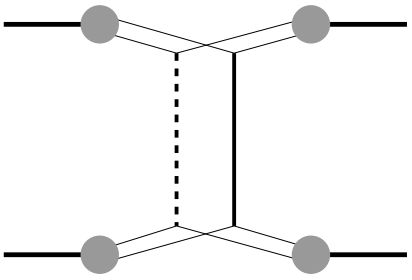

The squared amplitude is now the sum over many such terms represented by solid and dashed lines.

When squaring an amplitude being a sum of many terms, not all of the terms interfere – only those which correspond to the same final state. For example, a single inelastic interaction does not interfere with a double inelastic interaction, whereas all the contributions with exactly on inelastic interaction interfere. So considering a squared amplitude, one may group terms together representing

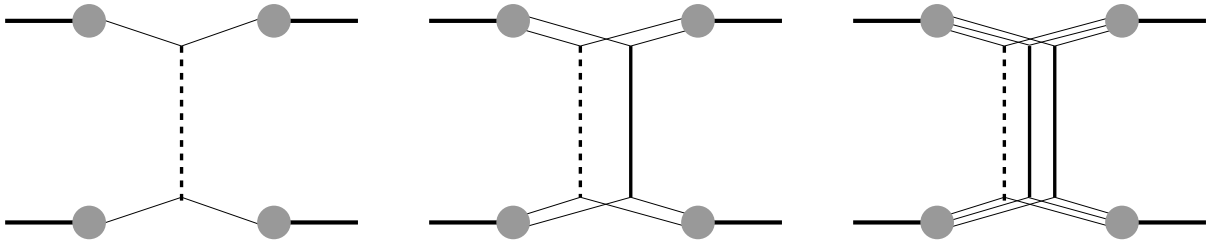

Figure **25**: Class of terms corresponding to one inelastic interaction.

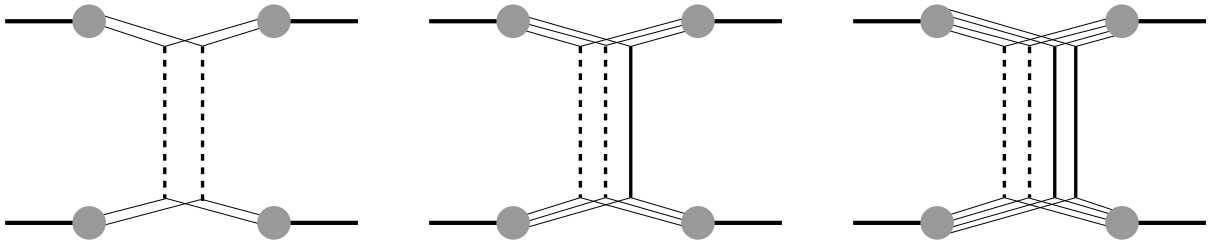

Figure **26**: Class of terms corresponding to two inelastic interactions.

the same final state. In our pictorial language, this means that all diagrams with one dashed line, representing the same final state, may be considered to form a class, characterized by $m = 1$ – one dashed line (one elementary cut) – and the light cone momenta x^+ and x^- attached to the dashed line (defining energy and momentum of the Pomeron). In fig. 25, we show several diagrams belonging to this class, in fig. 26, we show the diagrams belonging to the class of two inelastic interactions, characterized by $m = 2$ and four light-cone momenta x_1^+, x_1^-, x_2^+, x_2^-. Generalizing these considerations, we may group all contributions with m inelastic interactions (m dashed lines = m cut Pomerons) into a class characterized by the variable

$$K = \{m, x_1^+, x_1^-, \cdots, x_m^+, x_m^-\}.$$

We then sum all the terms in a class K,

$$\Omega(K) = \sum \{\text{all terms in class } K\}.$$

The cross section is then simply a sum over classes,

$$\sigma_{\text{inel}}(s) = \sum_{K \neq 0} \int d^2b \, \Omega(K).$$

Ω depends implicitly on the energy squared s and the impact parameter b: $\Omega = \Omega^{(s,b)}$. The individual terms $\int d^2b \, \Omega(K)$, represent partial cross sections, since they represent distinct final states. They are referred to as topological cross sections.

The above concepts are easily generalized to nucleus-nucleus scattering, an example for a diagram representing a contribution to the squared amplitude is shown in fig. 27. We may also define classes, which correspond to well defined

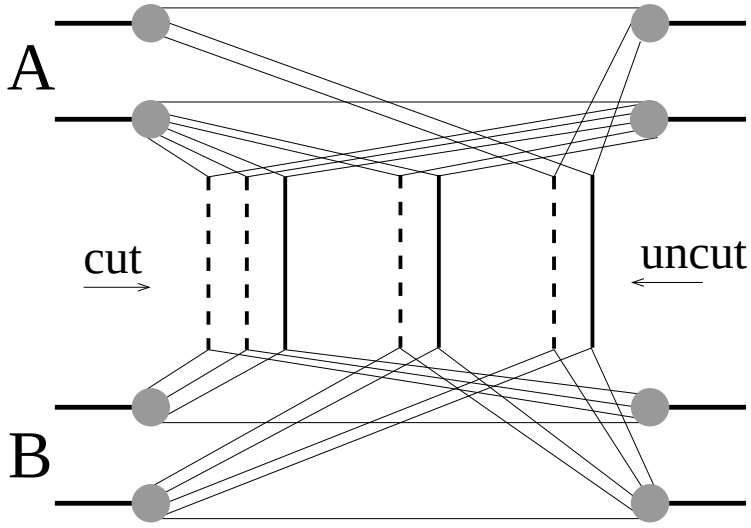

Figure **27**: Nucleus-nucleus collisions: A contribution to the squared amplitude.

final states, in our notation a given number of dashed lines between nucleon pairs. We may number the pairs as 1, 2, 3, ... k ... , AB. We define m_k to be the number of inelastic interactions (cut Pomerons) of the pair number k. The $\mu^{\rm th}$ of these m_k cut Pomerons is characterized by light cone momenta $x^+_{k\mu}$, $x^-_{k\mu}$. So a class may be characterized by

$$K = \{m_k, x^+_{k\mu}, x^-_{k\mu}\}.$$

We sum all terms in a class to obtain again a quantity called $\Omega^{(s,b)}(K)$, such that the cross section can be written as a sum over classes

$$\sigma_{\rm inel}(s) = \sum_{K\neq 0} \int d^2b\, \Omega^{(s,b)}(K),$$

as in the case of proton-proton scattering. Here, however, b is a multidimensional variable representing the impact parameter b_0 and the transverse distances b_k of all the nucleon-nucleon pairs,

$$b = \{b_0, b_1, ..., b_{AB}\}, \tag{14}$$

and $\int d^2b$ is a symbolic notation, meaning

$$\int d^2b = \int d^2b_0 \int \prod_{i=1}^{A} d^2b_i^A\, T_A(b_i^A) \prod_{j=1}^{B} d^2b_j^B\, T_B(b_j^B), \tag{15}$$

with A, B being the nuclear mass numbers and with the so-called nuclear thickness function $T_A(b)$ being defined as the integral over the nuclear density $\rho_{A(B)}$,

$$T_A(b) := \int dz\, \rho_A(\sqrt{b^2+z^2}). \tag{16}$$

One can prove

$$\sum_K \Omega(K) = 1,$$

which is a very important result justifying our interpretation of $\Omega(K)$ to be a probability distribution for the configurations K. This provides also the basis for applying Monte Carlo techniques.

The function Ω is the basis of all applications of this formalism. It provides the basis for calculating (topological) cross sections, but also for particle production, thus providing a consistent formalism for all aspects of a nuclear collision.

For the sake of completeness, we provide the formula for Ω, expressed in terms of the elementary interactions G_k (indices k express that G depends on the considered pair because of ladder splitting correction) and some vertex function F [26]:

$$\Omega_{AB}^{(s,b)}(m, X^+, X^-) = \prod_{k=1}^{AB} \left\{ \frac{1}{m_k!} \prod_{\mu=1}^{m_k} G_k(x_{k,\mu}^+, x_{k,\mu}^-, s, b_k) \right\} \Phi_{AB}\left(x^{\rm proj}, x^{\rm targ}, s, b\right), \tag{17}$$

with a function Φ representing summations over all uncut contributions corresponding to a given cut configuration, given as

$$\begin{aligned} \Phi_{AB}\left(x^{\rm proj}, x^{\rm targ}, s, b\right) &= \sum_{l_1} \cdots \sum_{l_{AB}} \\ &\times \int \prod_{k=1}^{AB} \left\{ \prod_{\lambda=1}^{l_k} d\tilde{x}_{k,\lambda}^+ d\tilde{x}_{k,\lambda}^- \right\} \prod_{k=1}^{AB} \left\{ \frac{1}{l_k!} \prod_{\lambda=1}^{l_k} -G_k(\tilde{x}_{k,\lambda}^+, \tilde{x}_{k,\lambda}^-, s, b_k) \right\} \\ &\times \prod_{i=1}^{A} F_{\rm remn}\left(x_i^{\rm proj} - \sum_{\pi(k)=i} \tilde{x}_{k,\lambda}^+ \right) \prod_{j=1}^{B} F_{\rm remn}\left(x_j^{\rm targ} - \sum_{\tau(k)=j} \tilde{x}_{k,\lambda}^- \right). \end{aligned} \tag{18}$$

The different arguments are defined as

$$X^+ = \left\{ x_{k,\mu}^+ \right\}, \tag{19}$$

$$X^- = \left\{ x_{k,\mu}^- \right\}, \tag{20}$$

$$x^{\rm proj} = \left\{ x_i^{\rm proj} \right\}, \tag{21}$$

$$x^{\rm targ} = \left\{ x_j^{\rm targ} \right\}, \tag{22}$$

$$m = \{m_k\}, \tag{23}$$

and

$$x_i^{\rm proj} = 1 - \sum_{\pi(k)=i} x_{k,\mu}^+, \tag{24}$$

$$x_j^{\rm targ} = 1 - \sum_{\tau(k)=j} x_{k,\mu}^- . \tag{25}$$

The functions $\pi(k)$ and $\tau(k)$ refer to the projectile and the target nucleons participating in the $k^{\rm th}$ interaction (pair k) and $F_{\rm remn}$ is the vertex function to the projectile or target remnant.

B Appendix on Soft and Hard Elementary Interactions

What are actually these G functions, which represent elementary interactions? To explain this we have to discuss some basic facts about scattering. Let T be the elastic scattering amplitude T for a $2 \to 2$ scattering. The 4-momenta p and p' are the ones for the incoming particles , $\tilde{p} = p + q$ and $\tilde{p}' = p' - q$ the ones for the outgoing particles, and q the 4-momentum transfer in the process. We define as usual the Mandelstam variables s and t. Using the optical theorem, we may write the total cross section as

$$\sigma_{\rm tot}(s) = \frac{1}{2s} 2{\rm Im}\, T(s, t = 0). \tag{26}$$

We define the Fourier transform $\tilde{T}$ of T as

$$\tilde{T}(s, b) = \frac{1}{4\pi^2} \int d^2 q_\perp \, e^{-i\vec{q}_\perp \vec{b}} \, T(s, t), \tag{27}$$

using $t = -q_\perp^2$, and we define G as

$$G(s, b) = \frac{1}{2s} 2{\rm Im}\, \tilde{T}(s, b). \tag{28}$$

One can easily verify that

$$\sigma_{\rm tot}(s) = \int d^2 b \; G(s, b), \tag{29}$$

which allows an interpretation of $G(s, b)$ to be the probability of an interaction at impact parameter b.

This are actually such "G functions" which appear in the multiple scattering formulas. The fact that an elementary scattering of nucleon constituents (quarks) is composed of soft and hard components (and a semihard one, as discussed later) can be expressed as

$$G = G_{\rm soft} + G_{\rm hard}. \tag{30}$$

Soft Interactions

Let us first consider a soft interaction (with only small virtualities involved). We assume that nucleon constituents (quarks, diquarks,...) from projectile and target may interact with the result of producing many (low p_t) hadrons. We refer to this as an elementary soft interaction of nucleon constituents. The corresponding amplitude (T-matrix element) is assumed to be of the form

$$T_{\rm soft}(s, t) = i \, 8\pi \, s_0 \, \gamma_{\rm part}^2 \left(\frac{s}{s_0} \right)^{\alpha_{\rm soft}} \exp(\lambda_{\rm soft}(s/s_0) \, t) \, , \tag{31}$$

$$\lambda_{\rm soft}(z) = 2R_{\rm part}^2 + \alpha'_{\rm soft} \ln z, \tag{32}$$

with parameters $\alpha_{\rm soft}$, $\alpha'_{\rm soft}$, $\gamma_{\rm part}$, $R^2_{\rm part}$, and a scale $s_0 = 1{\rm GeV}^2$. We define $G_{\rm soft}(s,b)$ to be twice the imaginary part of the Fourier transform (with respect to $k_\perp = -t$) of $T_{\rm soft}$, as discussed above. We find

$$G_{\rm soft}(s,b) = \frac{2\gamma^2_{\rm part}}{\lambda_{\rm soft}(s/s_0)} \left(\frac{s}{s_0}\right)^{\alpha_{\rm soft}-1} \exp\left(-\frac{b^2}{4\lambda_{\rm soft}(s/s_0)}\right). \qquad (33)$$

Hard interactions

We now proceed to the case of hard scattering , being the other extreme, when all internal intermediate partons are characterized by large virtualities $Q^2 > Q_0^2$. Here, the corresponding amplitude $T^{jk}_{\rm hard}(s,t)$ of the scattering of two partons with flavors j and k can be calculated using the perturbative QCD techniques [27, 28]. In the leading logarithmic approximation of QCD, summing up terms where each (small) running QCD coupling constant $\alpha_s(Q^2)$ appears together with a large logarithm $\ln(Q^2/\lambda^2_{\rm QCD})$ (with λ_{QCD} being the infrared QCD scale), and making use of the factorization hypothesis, one obtains the contribution of the corresponding cut diagram for $t = q^2 = 0$ as the cut parton ladder cross section $\sigma^{jk}_{\rm hard}(s,Q_0^2)$ (strictly speaking, one obtains the ladder representation for the process only using axial gauge), where all horizontal rungs of the ladder are the final (on-shell) partons and the virtualities of the virtual t-channel partons increase from the ends of the ladder towards the largest momentum transfer parton-parton process. We have

$$\begin{aligned}
\sigma^{jk}_{\rm hard}(s,Q_0^2) &= \frac{1}{2s} 2{\rm Im}\, T^{jk}_{\rm hard}(s,t=0) \\
&= K \sum_{ml} \int dx_B^+ dx_B^- dp_\perp^2 \frac{d\sigma^{ml}_{\rm Born}}{dp_\perp^2}(x_B^+ x_B^- s, p_\perp^2) \qquad (34) \\
&\times \; E^{jm}_{\rm QCD}(x_B^+, Q_0^2, M_F^2)\, E^{kl}_{\rm QCD}(x_B^-, Q_0^2, M_F^2) \theta\big(M_F^2 - Q_0^2\big)\,,
\end{aligned}$$

Here $d\sigma^{ml}_{\rm Born}/dp^2_\perp$ is the differential $2 \to 2$ parton scattering cross section, $p^2_\perp$ is the parton transverse momentum in the hard process, m, l and $x_B^\pm$ are correspondingly the types and the shares of the light cone momenta of the partons participating in the hard process, and M_F^2 is the factorization scale for the process (we use $M_F^2 = p_\perp^2/4$). The 'evolution function' $E^{jm}_{\rm QCD}(Q_0^2, M_F^2, z)$ represents the evolution of a parton cascade from the scale Q_0^2 to M_F^2, i.e. it gives the number density of partons of type m with the momentum share z at the virtuality scale M_F^2, resulted from the evolution of the initial parton j, taken at the virtuality scale Q_0^2. The evolution function satisfies the usual DGLAP equation [29–32] with the initial condition $E^{jm}_{\rm QCD}(Q_0^2, Q_0^2, z) = \delta^j_m\ \delta(1-z)$. The factor $K \simeq 1.5$ takes effectively into account higher order QCD corrections.

In the following we shall need to know the contribution of the uncut parton ladder $T^{jk}_{\rm hard}(s,t)$ with some momentum transfer q along the ladder (with $t = q^2$). The behavior of the corresponding amplitudes was studied in [33] in the leading logarithmic($1/x$) approximation of QCD. The precise form of the corresponding

amplitude is not important for our application; we just use some of the results of [33], namely that one can neglect the real part of this amplitude and that it is nearly independent on t, i.e. that the slope of the hard interaction $R^2_{\rm hard}$ is negligible small, i.e. compared to the soft Pomeron slope one has $R^2_{\rm hard} \simeq 0$. So we parameterize $T^{jk}_{\rm hard}(s,t)$ in the region of small t as [34]

$$T^{jk}_{\rm hard}(s,t) = is\,\sigma^{jk}_{\rm hard}(s,Q_0^2)\,\exp\left(R^2_{\rm hard}\,t\right), \tag{35}$$

The corresponding "G function" is obtained by calculating the Fourier transform $\tilde{T}$ of T and dividing by the initial parton flux $2\hat{s}$,

$$G^{jk}_{\rm hard}(s,b) = \frac{1}{2s} 2{\rm Im}\tilde{T}^{jk}_{\rm hard}(s,b), \tag{36}$$

which gives

$$G^{jk}_{\rm hard}\,(s,b) = \frac{1}{8\pi^2 s}\int d^2q_\perp\,\exp\Big(-i\vec{q}_\perp\vec{b}\Big)\;2{\rm Im}\,T^{jk}_{\rm hard}(s,-q_\perp^2),$$

or explicitly

$$G^{jk}_{\rm hard}\,(s,b) == \sigma^{jk}_{\rm hard}\big(s,Q_0^2\big)\,\frac{1}{4\pi R^2_{\rm hard}}\exp\left(-\frac{b^2}{4R^2_{\rm hard}}\right). \tag{37}$$

This is not yet the hard G function we are looking for, there is still one element missing, namely the relation between the partons j and k and the incident nucleons. There are two elements relevant: the vertex function, and the soft pre-evolution.

The vertex function

The coupling of the multiple (say n) elementary interactions to the nucleons is expressed via projectile and target nucleon vertex functions, having the form

$$F^N_{\rm remn}\left(1-\sum_{k=1}^{n}x_k\right)\;\exp\left(-R_N^2\sum_{k=1}^{n}q^2_{k_\perp}\right)\;\prod_{k=1}^{n}F^N_{\rm part}(x_k)\,, \tag{38}$$

with

$$F^N_{\rm part}(x) = \gamma_N\,x^{-\alpha_{\rm part}}, \tag{39}$$

$$F^N_{\rm remn}(x) = x^{\alpha^N_{\rm remn}}\,\Theta\,(x)\;\Theta\,(1-x)\,, \tag{40}$$

with parameters R_N^2, γ_N, $\alpha_{\rm part}$, $\alpha^N_{\rm remn}$. All parameters with an "N" sub(super)script are specific for projectile/target nucleons and may be different for other kinds of hadrons, like pions, kaons. The arguments x_k and $q^2_{k_\perp}$ are respectively the light cone momentum fractions and squared transverse momenta of the nucleon constituents participating in an interaction. All factors apart of $F_{\rm remn}$ can be absorbed into the elementary G functions.

Soft pre-evolution

In case of sea quarks and gluons being at the end of a parton ladder, the momentum share x_1 of the "first" parton is typically very small, leading to an object with a large mass of the order Q_0^2/x_1 between the parton and the proton [35]. Microscopically, such 'slow' partons with $x_1 \ll 1$ appear as a result of a long non-perturbative parton cascade, where each individual parton branching is characterized by a small momentum transfer squared $Q^2 < Q_0^2$ and nearly equal partition of the parent parton light cone momentum [36, 37]. When calculating proton structure functions or high-p_t jet production cross sections, this non-perturbative contribution is usually included into parameterized initial parton momentum distributions at $Q^2 = Q_0^2$. However, the description of inelastic hadronic interactions requires to treat it explicitly in order to account for secondary particles produced during such non-perturbative parton pre-evolution, and to describe correctly energy-momentum sharing between multiple elementary scatterings. As the underlying dynamics appears to be identical to the one of soft parton-parton scattering considered above, we treat this soft pre-evolution as the usual soft emission. We account for this by introducing "soft pre-evolutions functions" $E_{\rm soft}$, as discussed in more detail later.

The complete hard contribution

The complete G function, including soft pre-evolution and vertex contributions, is given as

$$
\begin{aligned}
G_{\rm hard}\left(x^+,x^-,s,b\right) \;&=\; F^N_{\rm part}(x^+)\,F^N_{\rm part}(x^-) \\
&\sum_{jk}\int_0^1 dz^+dz^-E^j_{\rm soft}\left(z^+\right)\,E^k_{\rm soft}\left(z^-\right)\,\sigma^{jk}_{\rm hard}(z^+z^-x^+x^-s,Q_0^2) \\
&\frac{1}{4\pi\,\lambda_{NN}(1/(z^+z^-))}\exp\left(-\frac{b^2}{4\lambda_{NN}(1/(z^+z^-))}\right)
\end{aligned}
\tag{41}
$$

with $\lambda_{NN}(\xi) = 2R_N^2 + \alpha'_{\rm soft}\ln\xi$. The variables x^+, x^- refer to the soft nucleon constituents participating in an elementary interaction. The variables z^+, z^- refer to the first hard partons, the ladder ends. The function $E^k_{\rm soft}$ has two contributions,

$$
E^k_{\rm soft}(z) = E^k_{\rm soft(0)}(z) + E^k_{\rm soft(1)}(z). \tag{42}
$$

The first term, representing a soft "pre-evolution", is given as ${\rm Im}T_{\rm soft}(s_0/z, t=0)$, up to some coupling modifications, explicitely

$$
E^q_{\rm soft(0)}(z) = z^{-\alpha_{\rm soft}}\,\tilde{E}^q_{\rm soft(0)}(z), \quad E^g_{\rm soft(0)}(z) = z^{-\alpha_{\rm soft}}\,\tilde{E}^g_{\rm soft(0)}(z), \tag{43}
$$

with

$$
\tilde{E}^q_{\rm soft(0)}(z) = \gamma_{\rm soft}\,w\,\hat{E}^q_{\rm soft(0)}(z), \quad \tilde{E}^g_{\rm soft(0)}(z) = \gamma_{\rm soft}\,(1-w)\,(1-z)^\beta, \tag{44}
$$

with $\gamma_{\rm soft} = 8\pi s_0\gamma_{\rm part}\tilde{\gamma}$, and

$$
\hat{E}^q_{\rm soft(0)}(z) = \int_x^1 d\xi\,\xi^{\delta_s}\,P(\xi)\,(1-\frac{z}{\xi})^\beta, \tag{45}
$$

with some parameters $\tilde{\gamma}$ and β.

The second term, representing a direct coupling to a valence quark, and which has therefore only a quark contribution, can be written as

$$E^q_{\mathrm{soft}(1)}(x,z) = z^{-\alpha_{\mathrm{soft}}}\, \tilde{E}^q_{\mathrm{soft}(1)}(z\,x,x), \tag{46}$$

with

$$\begin{aligned}\tilde{E}^q_{\mathrm{soft}(1)}(x_q,x) &= x\,\frac{1}{\gamma_h} x^{\alpha_{\mathrm{part}}} \frac{\Gamma(2+\alpha_{\mathrm{remn}}-\alpha_{\mathbb{R}})}{\Gamma(1+\alpha_{\mathrm{remn}})\Gamma(1-\alpha_{\mathbb{R}})} \\ &\quad q_{\mathrm{val}}(x_q)(1-x_q)^{-1-\alpha_{\mathrm{remn}}+\alpha_{\mathbb{R}}}(x-x_q)^{-\alpha_{\mathbb{R}}}.\end{aligned} \tag{47}$$

So this function depends also on the momentum fraction x. We neglected the small hard scattering slope R^2_{hard} compared to the Pomeron slope λ_{soft}.

We call E_{soft} also the " soft evolution", to indicate that we consider this as simply a continuation of the QCD evolution, however, in a region where perturbative techniques do not apply any more. $E^j_{\mathrm{soft}}(z)$ has the meaning of the momentum distribution of parton j in the soft piece. More details can be found in [26].

C Appendix on Parameterizations of G Functions

The calculations of partial cross sections in our multiple scattering theory involve high dimensional integrations, excluding numerical techniques. Fortunately, the numerically determined G function (the sum of soft and hard) can to a high precision be expressed as

$$G(x^+,x^-,s,b) = (x^+x^-)^{-\alpha_{\mathrm{part}}} \sum_{i=1}^{2} \alpha_{G_i}\, s^{\beta_{G_i}}\, (x^+x^-)^{\beta'_{G_i}}\, (sx^+x^-)^{\gamma_{G_i}b^2} \exp(-\frac{b^2}{\delta_{G_i}}). \tag{48}$$

This form is inspired by the fact that G is a sum of two contributions, soft ($i=1$) and hard ($i=2$), with quite different exponents β'_{G_i}. The fit parameters are, however, chosen such that the sum of both, soft and hard, is best reproduced. The above form provides in fact excellent fits of the x^+, x^-, and also the b dependence of G. Concerning this b dependence, one has

$$(sx^+x^-)^{\gamma_{G_i}b^2} \exp(-\frac{b^2}{\delta_{G_i}}) \approx \exp(-\frac{b^2}{\lambda_{G_i}}), \tag{49}$$

with

$$\lambda_{G_i} = \delta_{G_i} + \delta^2_{G_i}\gamma_{G_i} \ln(sx^+x^-), \tag{50}$$

indicating that the width of the b dependence increases logarithmically with energy.

Using the analytical form of G, many of the multidimensional integrals can be done analytically. For a given s and b, one may write

$$G(x^+,x^-,s,b) = \sum_{i=1}^{2} \alpha_i\, (x^+x^-)^{\beta_i}, \tag{51}$$

with s and b dependent coefficients α_i, β_i. We also use the notation $\beta_S \equiv \beta_1$ and $\beta_H \equiv \beta_2$. Taking into account screening via the exponents $\varepsilon_S \equiv \varepsilon_1$ and $\varepsilon_H \equiv \varepsilon_2$ (see section 4), we have

$$G(x^+, x^-, s, b) = \sum_{i=1}^{2} \alpha_i \, (x^+)^{\beta_i + \varepsilon_i(Z_P)} \, (x^-)^{\beta_i + \varepsilon_i(Z_T)}. \tag{52}$$

The first task is the calculation of the function Φ, representing summations over all uncut contributions corresponding to a given cut configuration, which we need to know to be able to calculate partial cross section. For nucleon-nucleon, one obtains

$$\Phi_{NN}(x^+, x^-, s, b) = (x^+ x^-)^{\alpha_{\rm remn}} \sum_{i=0}^{\infty} \sum_{j=0}^{\infty} \frac{(a_1)^i}{i!} \, \frac{(a_2)^j}{j!} \, g(i\tilde{\beta}_1 + j\tilde{\beta}_2) \, g(i\tilde{\beta}'_1 + j\tilde{\beta}'_2), \tag{53}$$

with $a_i = -\alpha_i \Gamma(\tilde{\beta}_i)\Gamma(\tilde{\beta'}_i)(x^+)^{\tilde{\beta}_i}(x^-)^{\tilde{\beta'}_i}$, and $\tilde{\beta}_i = \beta_i + \varepsilon_i(Z_P) + 1$, $\tilde{\beta}'_i = \beta_i + \varepsilon_i(Z_T) + 1$. The function g is given as

$$g(x) = \frac{\Gamma(1 + \alpha_{\rm remn})}{\Gamma(1 + \alpha_{\rm remn} + x)} \, .$$

Φ_{NN} is almost an exponential function. So to regularize the theory, we replace $g(i\tilde{\beta}_1 + j\tilde{\beta}_2)$ by $g(\tilde{\beta}_1)^i g(\tilde{\beta}_2)^j$, to get an exponential-type function. It is not precisely the same, but we take this freedom, because even small deviations from an exponential form of Φ may lead to drastic consequences (big oscillations), not at all being physical. All these considerations can be generalized to nucleus-nucleus (AB) collisions, where we have to evaluate Φ_{AB}. One gets

$$\begin{aligned} \Phi_{AB}(x^{\rm proj}, x^{\rm targ}, s, b) &= \prod_{k=1}^{AB} \exp\Big(-\tilde{G}_k(x^+_{\pi(k)}, x^-_{\tau(k)}, s, b_k)\Big) \\ &\times \prod_{i=1}^{A} (x_i^+)^{\alpha_{\rm remn}} \, \Theta(x_i^+) \, \Theta(1 - x_i^+) \prod_{j=1}^{B} (x_j^-)^{\alpha_{\rm remn}} \, \Theta(x_j^-) \, \Theta(1 - x_j^-), \end{aligned} \tag{54}$$

with

$$\tilde{G}_k(x^+, x^-, s, b) = \sum_{i=1}^{2} \tilde{\alpha}_i^k \, (x^+)^{\tilde{\beta}_i^k} \, (x^-)^{\tilde{\beta'}_i^k}, \tag{55}$$

with

$$\tilde{\alpha}_i^k = \alpha_i^k \, \frac{\Gamma(\tilde{\beta}_i^k)\Gamma(1 + \alpha_{\rm remn})}{\Gamma(1 + \alpha_{\rm remn} + \tilde{\beta}_i^k)} \, \frac{\Gamma(\tilde{\beta'}_i^k)\Gamma(1 + \alpha_{\rm remn})}{\Gamma(1 + \alpha_{\rm remn} + \tilde{\beta'}_i^k)}, \tag{56}$$

$$\tilde{\beta}_i^k = \beta_i^k + \varepsilon_i(Z_P) + 1, \tag{57}$$

$$\tilde{\beta'}_i^k = \beta_i^k + \varepsilon_i(Z_T) + 1, \tag{58}$$

with

$$\alpha_i^k = \alpha_{G_i} \exp(-\frac{b_k^2}{\delta_{G_i}}) \, s^{\beta_{G_i} + \gamma_{G_i} b_k^2}, \tag{59}$$

$$\beta_i^k = \beta'_{G_i} + \gamma_{G_i} b_k^2 - \alpha_{\rm part}. \tag{60}$$

More details can be found in [26].

D Appendix on Markov Chain Techniques

As discussed earlier, the function Ω (the integrand of partial cross sections) can be interpreted as probability distribution, which allows to apply the Monte Carlo technique. So we want to generate configurations $\{m, X^+, X^-\}$ according to

$$\Omega_{AB}^{(s,b)}(m, X^+, X^-) = \prod_{k=1}^{AB} \left\{ \frac{1}{m_k!} \prod_{\mu=1}^{m_k} G_k(x_{k,\mu}^+, x_{k,\mu}^-, s, b_k) \right\} \Phi_{AB}\left(X^{\rm proj}, X^{\rm targ}, s, b\right), \qquad (61)$$

with

$$b = \{b_k\},\ m = \{m_k\},\ X^+ = \left\{x_{k,\mu}^+\right\},\ X^- = \left\{x_{k,\mu}^-\right\},\ X^{\rm proj} = \left\{x_i^{\rm proj}\right\},\ X^{\rm targ} = \left\{x_j^{\rm targ}\right\}, \qquad (62)$$

Here, b_0 is the impact parameter between the two nuclei, and b_k is the transverse distance between the nucleons of k^{th} pair, m_k is the number of elementary inelastic interaction for the nucleon-nucleon pair k, $x_{k,\mu}^+$ and $x_{k,\mu}^-$ are the light cone momenta of the $\mu^{\rm th}$ interaction of the pair k. The arguments of Φ are the number of inelastic interactions m and the momentum fractions of projectile and target remnants,

$$x_i^{\rm proj} = 1 - \sum_{\pi(k)=i} x_{k,\mu}^+, \quad x_j^{\rm targ} = 1 - \sum_{\tau(k)=j} x_{k,\mu}^-, \qquad (63)$$

where $\pi(k)$ and $\tau(k)$ point to the remnants linked to the $k^{\rm th}$ interaction. In the following, we perform the analysis for given s and $b = (b_0, b_1, ..., b_{AB})$, so we do not write these variables explicitly. Furthermore, we suppress the index AB. For any given configuration the function Ω can be easily calculated, using the techniques developed earlier.

Since $\Omega(m, X^+, X^-)$ is a high-dimensional and nontrivial probability distribution, the only way to proceed amounts to employing dynamical Monte Carlo methods, well known in statistical and solid state physics. We first need to choose the appropriate framework for our analysis. So we translate our problem into the language of spin systems [38]: we number all nucleon pairs as 1, 2, ..., AB and for each nucleon pair k the possible elementary interactions as 1,2, ..., m_k. Let $m_{\rm max}$ be the maximum number of elementary interactions per nucleon pair one may imagine. We now consider a two dimensional lattice with AB lines and $m_{\rm max}$ columns, see fig. 28. Lattice sites are occupied $(= 1)$ or empty $(= 0)$, representing an elementary interaction (1) or the case of no interaction (0), for the k^{th} pair. In order to represent m_k elementary interactions for the pair k, we need m_k occupied cells (1's) in the k^{th} line. A line containing only empty cells (0's) represents a pair without interaction. Any possible interaction may be represented by this "interaction matrix" M with elements

$$m_{kn} \in \{0, 1\}. \qquad (64)$$

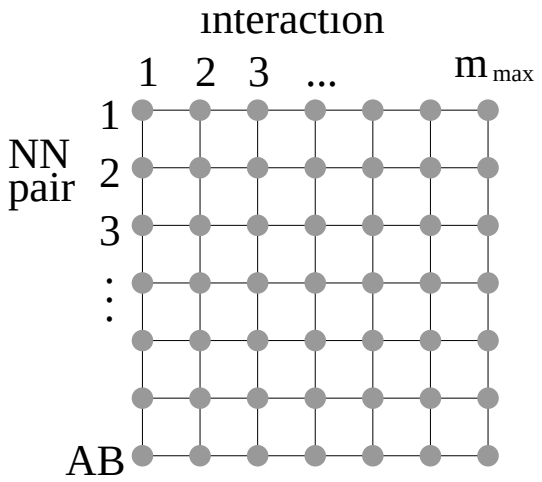

Figure **28**: The interaction lattice.

Such an "interaction configuration" is exactly equivalent to a spin configuration of the Ising model. Unfortunately the situation is somewhat more complicated in case of nuclear collisions: we need to consider the energy available for each elementary interaction, represented via the momentum fractions x^+_{kn} and x^-_{kn}. So we have a "generalized" matrix $K = (M, X^+, X^-)$, representing an interaction configuration. Since there are

$$c = \prod_{k=1}^{AB} \frac{m_{\max}!}{m_k!(m_{\max} - m_k)!} \tag{65}$$

configurations (M, X^+, X^-) representing the same configuration (m, X^+, X^-), the weight for the former is c^{-1} times the weight for the latter, so we obtain the following probability distribution for $K = (M, X^+, X^-)$:

$$\Omega(K) = \prod_{k=1}^{AB} \left\{ \frac{(m_{\max} - m_k)!}{m_{\max}!} \prod_{n=1}^{m_{\max}} \delta_{m_{kn}1}\, G_k(x^+_{kn}, x^-_{kn}, s, b) \right\} \Phi_{AB}\left(X^{\text{proj}}, X^{\text{targ}}, s, b\right). \tag{66}$$

In order to generate K according to the given distribution $\Omega(K)$, defined earlier, we construct a chain of configurations $K^{(t)}$ such that the final configurations $K^{(t_{\max})}$ are distributed according to the probability distribution $\Omega(K)$, if possible for a $t_{\max}$ not too large! Let us discuss how to obtain a new configuration $K^{(t+1)} = L$ from a given configuration $K^{(t)} = K$. We use Metropolis' Ansatz for the transition probability

$$p(K, L) = prob\left(K^{(t+1)} = L \,\middle|\, K^{(t)} = K\right) \tag{67}$$

as a product of a proposition matrix $w(K, L)$ and an acceptance matrix $u(K, L)$, where we use

$$u(K, L) = \min\left(\frac{\Omega(L)}{\Omega(K)} \frac{w(L, K)}{w(K, L)}, 1\right), \tag{68}$$

in order to assure detailed balance. We use

$$w(K, L) = \begin{cases} \Omega_0(L) & \text{if} \quad d(K, L) \leq 1 \\ 0 & \text{otherwise} \end{cases}, \tag{69}$$

where $d(K,L)$ is the number of lattice sites being different in L compared to K, and where Ω_0 is defined by the same formulas as Ω with one exception : Φ is replaced by $\prod_{k=1}^{AB}\prod_{n=1}^{m_{\max}}\delta_{m_{kn}1}\left(1-x_{kn}^{+}\right)\left(1-x_{kn}^{-}\right)$. So we get

$$\begin{aligned}\Omega_0(L) \;&\sim\; \prod_{k=1}^{AB}\Big\{\,(m_{\max}-m_k)! \\ &\times\; \prod_{n=1}^{m_{\max}}\delta_{m_{kn}1}\,G(x_{kn}^{+},x_{kn}^{-},s,b_k)\left(1-x_{kn}^{+}\right)\left(1-x_{kn}^{-}\right)\,\Big\}.\end{aligned} \tag{70}$$

The above definition of $w(K,L)$ may be realized by the following algorithm:

- ☐ choose randomly a lattice site (k,n),
- ☐ propose a new matrix element $(m_{kn},x_{kn}^{+},x_{k,n}^{-})$ according to the probability distribution $\rho(m_{kn},x_{kn}^{+},x_{k,n}^{-})$,

where we are going to derive the form of ρ in the following. From eq. (70), we know that ρ should be of the form

$$\rho(m,x^{+},x^{-}) \sim m_0!\begin{cases} G(x^{+},x^{-},s,b)\,(1-x^{+})\,(1-x^{-}) & \text{if}\quad m=1 \\ 1 & \text{if}\quad m=0 \end{cases}, \tag{71}$$

where $m_0 = m_{\max}-m$ is the number of zeros in the row k. Let us define $\bar{m}_0$ as the number of zeros (empty cells) in the row k not counting the current site (k,μ). Then the factor $m_0!$ is given as $\bar{m}_0!$ in case of $m\neq 0$ and as $\bar{m}_0!(\bar{m}_0+1)$ in case of $m=0$, and we obtain

$$\rho(m,x^{+},x^{-}) \sim (\bar{m}_0+1)\delta_{m0} + G(x^{+},x^{-},s,b)\left(1-x^{+}\right)\left(1-x^{-}\right)\delta_{m1}. \tag{72}$$

Properly normalized, we obtain

$$\rho(m,x^{+},x^{-}) = p_0\,\delta_{m0} + (1-p_0)\,\frac{G(x^{+},x^{-},s,b)\,(1-x^{+})\,(1-x^{-})}{\chi}\,\delta_{m1}, \tag{73}$$

where the probability p_0 of proposing no interaction is given as

$$p_0 = \frac{\bar{m}_0+1}{\bar{m}_0+1+\chi(s,b)}, \tag{74}$$

with χ being obtained by integrating $G(1-x^{+})(1-x^{-})$ over x^{+} and x^{-},

$$\chi(s,b) = \int_0^1 dx^{+}dx^{-}G(x^{+},x^{-},s,b)\left(1-x^{+}\right)\left(1-x^{-}\right). \tag{75}$$

Having proposed a new configuration L, which amounts to generating the values m_{kn}, x_{kn}^{+}, x_{kn}^{-} for a randomly chosen lattice site as described above, we accept this proposal with the probability

$$u(K,L) = \min\left(z_1 z_2, 1\right), \tag{76}$$

with

$$z_1 = \frac{\Omega(L)}{\Omega(K)}, \quad z_2 = \frac{w(L,K)}{w(K,L)}. \tag{77}$$

Since K and L differ in at most one lattice site, say (k,n), we do not need to evaluate the full formula for the distribution Ω to calculate z_1, we rather calculate

$$z_1 = \frac{\Omega^{kn}(L)}{\Omega^{kn}(K)}, \tag{78}$$

with

$$\begin{aligned} \Omega^{kn}(K) &= \big((\bar{m}_0+1)\delta_{m_{kn}0} + \delta_{m_{kn}1}\, G_k(x^+_{kn}, x^-_{kn}, s, b_k)\big) \\ &\times \exp\left(-\sum_{l \text{ linked to } k} \tilde{G}_l(x^{\text{proj}}_{\pi(l)}, x^{\text{targ}}_{\tau(l)}, s, b_l)\right) \\ &\times (x^{\text{proj}}_{\pi(k)})^{\alpha_{\text{remn}}}\Theta(x^{\text{proj}}_{\pi(k)})\Theta(1-x^{\text{proj}}_{\pi(k)})\,(x^{\text{targ}}_{\tau(k)})^{\alpha_{\text{remn}}}\Theta(x^{\text{targ}}_{\tau(k)})\Theta(1-x^{\text{targ}}_{\tau(k)}), \end{aligned} \tag{79}$$

which is technically quite easy. Our final task is the calculation of the asymmetry z_2. In many applications of the Markov chain method one uses symmetric proposal matrices, in which case this factor is simply one. This is not the case here. We have

$$z_2 = \frac{\Omega_0(K)}{\Omega_0(L)} = \frac{\Omega_0^{kn}(K)}{\Omega_0^{kn}(L)}, \tag{80}$$

with

$$\Omega_0^{kn}(K) = \rho(m_{kn}, x^+_{kn}, x^-_{kn}), \tag{81}$$

which is also easily calculated. So we accept the proposal L with the probability $\min(z_1 z_2, 1)$, in which case we have $K^{(t+1)} = L$, otherwise we keep the old configuration K, which means $K^{(t+1)} = K$.

References

[1] STAR collaboration, J. Adams et al., Phys.Rev.Lett. 91, 172302, 2003

[2] PHENIX collaboration, S. S. Adler et al., Phys. Rev. C 69, 034910 (2004)

[3] PHENIX collaboration, S. S. Adler et al., Phys. Rev. C 69, 034909 (2004)

[4] STAR collaboration, J. Adams et al., Phys. Rev. C70, 064907, 2004

[5] STAR collaboration, J. Adams et al., Phys. Rev. Lett. 91, 072304, 2003

[6] PHENIX collaboration, S.S. Adler et al., Phys. Rev. Lett. 91, 072303, 2003

[7] BRAHMS collaboration, I. Arsene et al., Phys. Rev. Lett. 93, 242303, 2004

[8] PHOBOS collaboration, B.B. Back et al., Phys. Rev. C70, 061901, 2004

[9] Dmitri Kharzeev, Eugene Levin, Larry McLerran, Nucl.Phys.A748: 627-640, 2005; D. Kharzeev, Y. V. Kovchegov and K. Tuchin, Phys. Rev. D 68, 094013, 2003

[10] R. Baier, A. Kovner and U. A. Wiedemann, Phys. Rev. D 68, 054009, 2003

[11] J. L. Albacete, N. Armesto, A. Kovner, C. A. Salgado and U. A. Wiedemann,Phys. Rev. Lett. 92, 082001, 2004

[12] J. Jalilian-Marian, Y. Nara and R. Venugopalan, Phys. Lett. B 577, 54, 2003;A. Dumitru and J. Jalilian-Marian, Phys. Rev. Lett. 89, 022301, 2002

[13] Rudolph C. Hwa,C.B. Yang, Phys.Rev.C70: 037901, 2004; Rudolph C. Hwa,C.B. Yang, Phys.Rev.C70: 054902, 2004.

[14] X.~N.~Wang, Phys. Lett. B 565, 116, 2003

[15] I.~Vitev, Phys. Lett. B 562, 36, 2003

[16] A. Accardi and M. Gyulassy, Phys. Lett. B 586, 244, 2004

[17] Z. W. Lin and C. M. Ko, Phys. Rev. C 68, 054904, 2003.

[18] M. Bleicher, F. M. Liu, A. Keränen, J. Aichelin, S.A. Bass, F. Becattini, K. Redlich, and K. Werner, Phys.Rev.Lett.88, 202501, 2002.

[19] F.M. Liu, J.Aichelin, M.Bleicher, H.J. Drescher, S. Ostapchenko, T. Pierog, and K. Werner, Phys. Rev. D67, 034011 (2003)

[20] UA5 collaboration, G.J. Alner et al., Z. Phys. C33, 1, 1986

[21] STAR collaboration, J. Adams et al., Phys. Rev. Lett. 91, 172302, 2003.

[22] PHENIX collaboration, Phys. Rev. Lett. 91, 241803

[23] PHOBOS collaboration , B.B. Back, Phys. Rev. Lett. 93, 082301, 2004

[24] BRAHMS collaboration, Phys. Rev. Lett. 94, 032301, 2005

[25] PHOBOS collaboration, nucl-ex/0409021, submitted to Phys. Rev. Lett.

[26] H. J. Drescher, M. Hladik, S. Ostapchenko, T. Pierog and K. Werner, Phys. Rept. 350, 93, 2001

[27] G. Altarelli, Phys. Rep. 81, 1, 1982.

[28] E. Reya, Phys. Rep. 69, 195, 1981.

[29] L. N. Lipatov, Sov. J. Nucl. Phys. 20, 94, 1975.

[30] V. N. Gribov and L. N. Lipatov, Sov. J. Nucl. Phys. 15, 438, 1972.

[31] G. Altarelli and G. Parisi, Nucl. Phys. B126, 298, 1977.

[32] Y. L. Dokshitzer, Sov. Phys. JETP 46, 641, 1977.

[33] L. N. Lipatov, Sov. Phys. JETP 63, 904, 1986.

[34] M. G. Ryskin and Y. M. Shabelski, Yad. Fiz., Rus. 55, 2149, 1992.

[35] A. Donnachie and P. Landshoff, Phys. Lett. B 332, 433, 1994.

[36] D. Amati, A. Stanghellini, and S. Fubini, Nuovo Cim. 26, 896, 1962.

[37] M. Baker and K. A. Ter-Martirosyan, Phys. Rep. 28, 1, 1976.

[38] M. Hladik, H. J. Drescher, S. Ostapchenko, T. Pierog, and K. Werner, Phys. Rev. Lett. 86, 3506, 2001